HHS Public Access

Author manuscript

J Immunol. Author manuscript; available in PMC 2023 January 15.

Published in final edited form as:

J Immunol. 2022 January 15; 208(2): 371–383. doi:10.4049/jimmunol.2100696.

Nemo-dependent, ATM-mediated signals from RAG DNA breaks at *Igk* feedback inhibit V_k recombination to enforce Igκ allelic exclusion

Rebecca A. Glynn[*,†], **Craig H. Bassing**[*,†,‡]

[*]Cell and Molecular Biology Graduate Group, Perelman School of Medicine, University of Pennsylvania, Philadelphia, PA, 19104

[†]Department of Pathology and Laboratory Medicine, Children's Hospital of Pennsylvania, Philadelphia, PA 19104

Abstract

Mono-allelic antigen receptor (AgR) gene expression underlies specific adaptive immune responses. AgR allelic exclusion is achieved by sequential initiation of V(D)J recombination between alleles and resultant protein from one allele signaling to prevent recombination of the other. The ATM kinase, a regulator of the DNA double strand break (DSB) response, helps enforce allelic exclusion through undetermined mechanisms. ATM promotes repair of RAG1/RAG2 (RAG) endonuclease-induced DSBs and transduces signals from RAG DSBs during *Igk* gene rearrangement on one allele to transiently inhibit RAG1 protein expression, *Igk* accessibility, and RAG cleavage of the other allele. Yet, the relative contributions of ATM functions in DSB repair versus signaling to enforce AgR allelic exclusion remain undetermined. Here, we demonstrate that inactivation in mouse pre-B cells of the NFκB essential modulator (Nemo) protein, an effector of ATM signaling, diminishes RAG DSB-triggered repression of *Rag1/Rag2* transcription and *Igk* accessibility, but does not result in aberrant repair of RAG DSBs like ATM inactivation. We show that Nemo deficiency increases simultaneous bi-allelic *Igk* cleavage in pre-B cells and raises the frequency of B cells expressing Igκ proteins from both alleles. In contrast, the incidence of bi-allelic Igκ expression is not elevated by inactivation of the SpiC transcriptional repressor, which is induced by RAG DSBs in an ATM-dependent manner and suppresses *Igk* accessibility. Thus, we conclude that Nemo-dependent, ATM-mediated DNA damage signals enforce Igκ allelic exclusion by orchestrating transient repression of RAG expression and feedback inhibition of additional *Igk* rearrangements in response to RAG cleavage on one *Igk* allele.

Introduction

In jawed vertebrates, most lymphocytes clonally express a unique antigen receptor (AgR), and collectively these cells display a diverse AgR repertoire that is essential for precise immune responses to an array of antigens. AgR diversity is generated through the somatic recombination of germline variable (V), diversity (D), and joining (J) gene segments

[‡]Corresponding Author: Craig H. Bassing, Ph.D., Children's Hospital of Philadelphia, 4054 Colket Translational Research Building, 3501 Civic Center Blvd., Philadelphia, PA 19104, 267-426-0311, bassing@chop.edu.

of immunoglobulin (Ig) and T cell receptor (TCR) genes in developing B and T cells, respectively. The lymphocyte-specific RAG1/RAG2 (RAG) endonuclease catalyzes V(D)J recombination by recognizing recombination signal sequences (RSSs) that flank all V, D, and J gene segments (1). As Ig or TCR loci become accessible, transcriptionally active, and topologically compacted, RAG binds over D or J RSSs and subsequently captures a compatible V or D RSS through diffusion-based collision or chromosome scanning (2–10). After this synapsis, RAG introduces a pair of DNA double strand breaks (DSBs) between each RSS and its flanking gene segment, generating two coding ends and two signal ends (1). RAG holds these ends in a post-cleavage synaptic complex, and the DSB response ATM kinase and non-homologous end-joining (NHEJ) DSB repair proteins stabilize these complexes, process the four DNA ends, and repair them to generate a coding join and signal join (11, 12). The coding join forms on the chromosome, producing a V(D)J rearrangement that encodes a variable region exon and resides upstream of constant (C) region exons needed for a complete Ig or TCR gene. The signal join typically forms on an extrachromosomal circle as most V(D)J rearrangements occur by deletion and excision of intervening sequences; however, signal joins also can form on the chromosome for the few types of V-to-(D)J rearrangements that proceed by inversion. The many possible permutations of V(D)J rearrangements and inherent imprecision in coding join formation cooperate to generate billions of distinct AgR genes. Although AgR gene assembly is critical for the health and survival of jawed vertebrate species, this process has life-threatening hazards for it inherently produces self-reactive receptors and can aberrantly create oncogenic genomic instability. Thus, cell intrinsic and extrinsic mechanisms control the initiation, completion, and outcomes of V(D)J recombination to limit these hazards (12–16).

V(D)J recombination and B and T cell development are interdependently regulated processes where signals direct AgR gene assembly in lymphocyte lineage-, developmental stage-, and allele-specific manners, and resultant AgR protein expression halts further rearrangements and drives continued differentiation (17). In the context of κ^+ B cell development within the bone marrow, common lymphoid progenitors differentiate into pro-B cells that arrest in the G1 cell cycle phase, induce RAG expression, and activate transcription, accessibility, and compaction of *Igh* loci (18). RAG binds over the J_H region, forming a recombination center (RC) that drives D_H-to-J_H recombination on both alleles and then captures a V_H segment for V_H-to-DJ_H recombination on one allele at a time (18). If the first VDJ_H join is out-of-frame, the cell can initiate either a replacement V_H rearrangement on the first allele or V_H-to-DJ_H recombination on the other allele until an in-frame join forms or the cell dies from apoptosis. When a VDJ_H join occurs in-frame, the resulting IgH protein binds the surrogate light chain λ5 and VpreB proteins to form a pre-B cell receptor (pre-BCR). This complex signals termination of RAG expression and implementation of epigenetic changes to enforce permanent feedback inhibition of V_H rearrangements on the other allele, ensuring mono-allelic expression (allelic exclusion) of IgH protein (18). Furthermore, pre-BCR signals in combination with IL7 receptor signaling promote differentiation and proliferation of pro-B cells to large cycling pre-B cells (19). For large pre-B cells to differentiate into small pre-B cells, IL7r signaling is attenuated by an increase in pre-BCR signaling and resulting induction of the CXCR4 receptor that,

upon stimulation by its ligand CXCL12, promotes escape from IL7 rich niches in the bone marrow to drive differentiation of small pre-B cells and cell cycle exit (20, 21). Upon arresting in G1, small pre-B cells induce RAG expression and fully activate transcription, accessibility, and compaction of *Igk* loci. RAG binds mainly over the J_k region to form a RC that captures a V_k segment for V_k-to-J_k recombination on one allele at a time (22). However, RAG also can bind over the V_k region to promote V_k-to-V_k rearrangements between V_k RSSs and overlapping RSSs of the opposite orientation (23). If the first VJ_k join is out-of-frame, the cell can attempt additional rearrangements on either allele until an in-frame join forms or the cell dies from apoptosis. When the VJ_k join is in-frame, the resulting Igκ protein can bind IgH protein to generate a κ^+ surface BCR that is selected based on its specificity for self-antigens within the bone marrow (24). If the BCR interacts weakly with self-antigens, it signals differentiation into κ^+ B cells and permanent feedback inhibition of V_k recombination through terminating RAG expression (24). As a result of permanent feedback inhibition, most κ^+ B cells exhibit mono-allelic IgH and Igκ expression and thus possess a BCR of a single unique specificity. Alternatively, if the BCR interacts strongly with self-antigens, it signals apoptosis, anergy, or an increase of RAG expression and additional *Igk* rearrangements that replace the existing VJ_k coding join (receptor editing) until an innocuous BCR is formed or *Igl* recombination initiates (24). During editing, V_k-to-J_k rearrangement can instead occur on the non-expressed *Igk* allele and create a distinct Igκ protein and a second BCR (25). This new BCR can signal differentiation, generating a κ^+ B cell with Igκ protein from both alleles (allelic inclusion) and thus two different antigen BCR specificities where one is self-reactive and an autoimmune hazard (25).

The precise mechanisms that govern allelic exclusion remain elusive (14, 26, 27). For receptor-mediated feedback inhibition to enforce allelic exclusion, only one allele can undergo V recombination within the time interval between initiation of recombination on one allele and receptor-mediated permanent silencing of the other allele. Epigenetic-based mechanisms have been proposed to orchestrate asynchronous initiation of V_k-to-J_k recombination between the two alleles (22, 28–31). Notably, these mechanisms do not explain what prevents the second allele from becoming accessible, being transcribed, and rearranging before a functional protein from the first allele signals permanent inhibition of *Igk* recombination. One proposed solution to this problem is that the process of V_k recombination on one allele activates transient feedback inhibition of recombination of the second allele (32). Consistent with this model, RAG DSBs induced on one *Igk* allele in primary pre-B cells signal via the ATM kinase to inhibit RAG cleavage of the other allele (33). During V(D)J recombination, ATM phosphorylates DSB repair proteins to stabilize RAG post-cleavage complexes and prevent end resection, promoting functional V(D)J coding join formation and suppressing oncogenic translocations (12, 34–37). In primary pre-B cells, inactivation of the ATM kinase allows RAG to cleave both *Igk* alleles in G1-arrested cells, and impairs the ability of RAG DSBs to signal downregulation of *Rag1* and *Rag2* (*Rag1/2*) transcript levels (33). These data formulated a model whereby RAG DSBs induced on one *Igk* allele signal through ATM to transiently suppress recombination by repressing *Rag1/2* expression (33). Consistent with this, ATM deficiency in mice increases bi-allelic assembly and expression of Igκ, as well as IgH and TCRβ (33, 37). In primary pre-B cells, ATM signaling from RAG DSBs also stimulates both canonical and non-canonical NFκB

transcription factor-dependent upregulation of many genes, including the Pim2 pro-survival kinase (a canonical target) and the SpiC transcriptional repressor (a non-canonical target) (38–40). When SpiC is constitutively and ectopically over-expressed in primary pre-B cells, it binds the 3' *Igk* enhancer to reduce transcription, accessibility, and RAG cleavage of J_k gene segments (40). Collectively, these data formulated a model whereby RAG DSBs on one *Igk* allele signal through ATM to transcriptionally repress *Rag1/2* expression and J_k accessibility, which would cooperate to suppress V_k-to-J_k rearrangements on the other allele until after the first allele is repaired (41). This RAG DSB-induced transient feedback inhibition model posits that ATM enforces allelic exclusion by signaling to prevent bi-allelic initiation of *Igk* recombination. However, as ATM promotes DSB repair, an additional and non-mutually exclusive explanation is that slower coding join formation in the absence of ATM extends the time interval between RAG cleavage on one allele and receptor-mediated permanent feedback inhibition of the other allele, thereby increasing the frequency of bi-allelic *Igk* assembly and expression (33).

To determine how ATM enforces Igκ allelic exclusion, we sought to inactivate ATM signals that suppress *Rag1/2* expression or J_k accessibility, while leaving unaffected ATM functions in DSB repair. The ability of ATM to induce gene expression changes in response to RAG DSBs at *Igk* loci depends on the NFκB essential modulator (Nemo) protein (38), for Nemo is necessary for stimulus-induced activation of canonical NFκB factors (42–44). As Nemo inactivation in pre-B cells impairs ATM-dependent repression of *Rag1/2* transcripts upon DSBs induced by ionizing radiation (45), we tested if Nemo also is needed for ATM signals that suppress *Rag1/2* expression and further *Igk* recombination in response to RAG cleavage of one *Igk* allele in primary pre-B cells. We demonstrate that Nemo inactivation increases bi-allelic RAG cleavage of *Igk* loci. We also show that RAG DSBs induced during *Igk* rearrangement signal repression of *Rag1/2* transcription, with this response diminished by Nemo deficiency. Moreover, we find that Nemo is required for RAG DSB-induced, ATM-dependent expression of the non-canonical NFκB factor-induced transcriptional repressor, SpiC, but SpiC deficiency has no effect on DSB-induced repression of *Rag1/2* expression. Finally, we show that inactivation of Nemo, but not SpiC, increases the frequency of mature B cells with bi-allelic Igκ protein expression as does ATM deficiency, yet Nemo deficiency does not impair V_k-J_k coding join formation similar to ATM inactivation. Collectively, our data demonstrate that Igκ allelic exclusion is enforced by Nemo-dependent, ATM-mediated signals induced by RAG DSBs on one *Igk* allele that transiently feedback inhibit V_k-to-J_k recombination on the other allele. Moreover, our finding that inactivation of SpiC alone does not increase bi-allelic Igκ protein expression reveals that disruption of RAG DSB-induced repression of J_k accessibility alone is not sufficient to disrupt Igκ allelic exclusion. Therefore, we propose that Nemo-dependent repression of *Rag1/2* transcription is a critical mechanism by which the ATM DSB response protein enforces Igκ allelic exclusion.

Materials and Methods

Mice

All mice used in this study were 4–6 weeks old, on a mixed 129SvEv and C57BL/6 background, of either sex, and housed under specific pathogen–free conditions at

the Children's Hospital of Philadelphia (CHOP). Animal husbandry, breeding, and experiments were performed in accordance with national guidelines and regulations and approved by the CHOP Institutional Animal Care and Use Committee. Experimental mice were euthanized by exposure to CO_2 followed by cervical dislocation. The *BCL2:IgH:Rag1*$^{-/-}$*:Nemo*$^{flox/flox}$ (*BIR1*), *Mb1Cre*$^{+}$*:BCL2:IgH:Rag1*$^{-/-}$*:Nemo*$^{flox/flox}$ (*BIR1:Nemo*$^{-/-}$), *BCL2:IgH:Artemis*$^{-/-}$*:Nemo*$^{flox/flox}$ (*BIA*), and *Mb1Cre*$^{+}$*:BCL2:IgH:Artemis*$^{-/-}$*:Nemo*$^{flox/flox}$ (*BIA:Nemo*$^{-/-}$) mice were generated by breeding previously described *BCL2:IgH:Rag1*$^{-/-}$ and *BCL2:IgH:Artemis*$^{-/-}$*:Nemo*$^{flox/flox}$ mice (39) with *Mb1Cre*$^{+}$*:Nemo*$^{flox/flox}$ mice (45). The *Mb1Cre*$^{+}$*:Nemo*$^{flox/flox}$, *Nemo*$^{flox/flox}$*:Igk*$^{m/h}$, *Mb1Cre*$^{+}$*:Nemo*$^{flox/flox}$*:Igk*$^{m/h}$, and *Spic*$^{-/-}$*:Nemo*$^{flox/flox}$*:Igk*$^{m/h}$, and *Atm*$^{-/-}$ mice were made by breeding together previously described *Mb1Cre*$^{+}$*:Nemo*$^{flox/flox}$ (45), *Mb1Cre*$^{+}$*:Atm*$^{flox/flox}$*:Igk*$^{m/h}$ (33), *Spic*$^{-/-}$ (46), and *Atm*$^{+/-}$ (37) mice. The wildtype control mice were littermate controls.

Ex vivo Primary Pre-B Cell Cultures

Primary bone marrow was harvested by flushing all leg bones of at least four mice of the appropriate genotype for each culture. These bone marrow cells were cultured for 4 days in RPMI 1640 supplemented with 10% FBS, 10 mM HEPES, 13 nonessential amino acids, 1 mM L-glutamine, 1 mM sodium pyruvate, 100 U/ml penicillin-streptomycin, 50 mM 2-ME, and 5 ng/ml IL7 (R&D Systems, 407-ML). Cells were plated at a density of 5 million cells per milliliter of media. After 2 days, cells were harvested and put back into culture in fresh IL7+ media at a density of 5 million cells per milliliter. After 4 days of culture, pre-B cells were sorted by depletion using EasySep™ mouse B cell isolation kit according to manufacturer's instructions (Stemcell Technologies). To induce G1 arrest and activate transcription of *Rag1* and *Rag2* and *Igk* recombination by IL7 withdrawal, we pelleted cells by centrifugation, resuspended them in the same media lacking IL7 at a density of 2 million cells per milliliter. Cells were harvested after 4 days in culture with IL7 and 24, 48, and 72 hours after IL7 withdrawal. Pre-B cell purity was assessed by flow cytometry at each collection time. Cells pellets were washed with PBS and split for either total RNA or J_k cleavage analysis. Where used, the ATM inhibitor KU55933 (Sigma-Aldrich, SML1109) was added to the IL7- media at the time of IL7 withdrawal to a concentration of 15μM.

Culturing Total Bone Marrow

Total bone marrow was flushed from all leg bones of individual mice of the appropriate genotype, depleted of red blood cells, pelleted by centrifugation, and resuspended at a density of approximately 10 million cells per milliliter in IL7- media used for the *ex vivo* primary pre-B cell cultures. The cells were split into 5 aliquots, one was collected as a baseline sample and the others were cultured for 1 or 4 hours after being treated with DMSO or 10 μg/mL of etoposide (Sigma-Aldrich, E2600000). The cells were collected in 1mL of TRIzol for RNA analysis.

Real-time PCR quantification of mRNA

For primary pre-B cell culture samples, three million cultured pre-B cells were harvested at indicated time points and immediately lysed in TRIzol (Life Technologies, 15596018). Total RNA was isolated using the RNeasy mini kit (Qiagen, 74106), treated with DNase (RNase-

Free DNase Set, Qiagen, 79254), and reverse transcribed to generate cDNA with High-Capacity RNA-to-cDNA™ Kit (Applied Biosystems, 4387406) according to manufacturer's directions. The cDNAs were then used as a template for real-time PCRs (RT-PCRs) performed with Power SYBR Green Master Mix (Applied Biosystems, 4367659) and run on a Quant Studio Flex 7 machine using the primers in Supplemental Table 1 for each corresponding transcript. Values were calculated by ΔΔCt analysis by first normalizing to *Cd19* as indicated, and then the indicated sample within each experiment.

Southern Blot and Quantification of Igk Cleavage

Southern blot analyses of RAG *Igκ* cleavage in primary pre-B cultures were performed as previously described (39) using 20 million cultured pre-B cells per sample. Quantification of the remaining GL J_k band was conducted using ImageJ software (National Institutes of Health).

Taqman Quantification of J_k Cleavage and Hybrid Joins

For primary pre-B cell culture samples, two million cultured pre-B cells were harvested at indicated time points and cell pellets were frozen until processing. To quantify hybrid join formation, sorted pre-B cells were pelleted and frozen until processing. Genomic DNA was isolated from cell pellets using the DNeasy Blood and Tissue Kit (Qiagen, 69506) according to the manufacturer's directions. Taqman assays were performed using 40–50ng of genomic DNA per sample, PrimeTime Gene Expression Master Mix (Integrated DNA Technologies, 1055772), and the corresponding primers in Supplemental Table 1 for each gene segment or hybrid join. The reactions were run on a Quant Studio Flex 7 machine and values were calculated by ΔΔCt analysis by first normalizing to the *Cd19* locus as indicated, and then the indicated sample for the J_k cleavage samples.

Click-IT Nascent Transcript Quantification

To analyze EU-labelled RNA in pre-B cell cultures, 8 million pre-B cells were diluted with additional IL7+ or IL7- media to 1 million cells/mL and treated with 0.5 mM 5-ethynyl uridine (EU, Life Technologies, E10345) for 1 hour prior to collection at the indicated time points. The cells were processed and the assays were conducted using the Click-It Nascent RNA Capture Kit (Life Technologies, C10365). RNA was isolated using TRIzol (Life Technologies) according to the manufacturer's instructions. Click-It chemistry and streptavidin pulldown of EU-labelled RNA were performed according to the Click-It Nascent RNA Capture kit's instructions. Pulled-down RNA was reverse transcribed using the Superscript VILO™ cDNA synthesis kit (Life Technologies, 11754–050) by the manufacturer's instructions and the cDNA was used as a template for RT-PCR as described earlier with the corresponding primers in Supplemental Table 1.

Flow Cytometry

Single cell suspensions were generated from the bone marrow and spleens of mice, depleted of red blood cells, and Fc receptors were blocked using anti-CD16/CD32 (BioLegend, 101302). Cells were stained with antibody panels in FACS buffer (PBS containing 2% FBS and 1mM EDTA), washed twice with FACS buffer, and then stained with LIVE/DEAD

Fixable Aqua Dead Cell Stain Kit (Invitrogen, L34957) in PBS. To evaluate the purity of pre-B cell cultures, a small aliquot of cells was taken at each time point collected and stained with BUV395 Rat anti-mouse CD45R/B220 (BD, 563793, Clone RA3–6B2), APC Rat anti-mouse CD43 (BD, 560663, Clone S7), and PE Rat anti-mouse IgM (eBioscience, 12-5790-81, Clone 11/41). Pre-B cells were gated by single, live, $B220^+$, $CD43^-$, and IgM^- cells and then small and large pre-B cells were determined using a side scatter by forward scatter plot. To assess apoptotic populations in the pre-B cell cultures, cells were stained with BUV395 Rat anti-mouse CD45R/B220 (BD, 563793, Clone RA3–6B2), APC Rat anti-mouse CD43 (BD, 560663, Clone S7), and APC Rat anti-mouse IgM (BD, 550676, Clone 11/41), and then stained with FITC Annexin V (BioLegend, 640905) in Annexin V Binding buffer (10mM HEPES, 140mM NaCl, and 35mM $CaCl_2$) and then propidium iodide solution (BioLegend, 421301) in FACS Buffer. Apoptotic populations were evaluated by gating on single, $B220^+$, $CD43^-$, IgM^- cells, then determining the small and large pre-B cells based on forward and side scatter, and then identifying the live, early apoptotic, late apoptotic, and necrotic populations using a FITC vs PE plot. To measure Igκ allelic inclusion, cells were stained with BUV395 Rat anti-mouse CD45R/B220 (BD, 563793, Clone RA3–6B2), APC Rat anti-mouse CD43 (BD, 560663, Clone S7), PE Rat anti-mouse Igκ light chain (BD, 559940, Clone 187.1), and FITC Goat anti-human Kappa (SouthernBiotech, 2061–02). Igκ positive populations were gated on lymphocytes, single, live, $B220^+$, $CD43^-$ cells. Data were collected on a LSRFortessa and analyzed with FlowJo software (Treestar). To evaluate hybrid join formation in pre-B cells, cells were stained in PE Rat anti-mouse CD45R/B220 (BD, 553090, Clone RA3–6B2), APC Rat anti-mouse CD43 (BD, 560663, Clone S7), and BV786 Rat anti-mouse IgM (BD, 743328, Clone 11/41). Cells were first gated on lymphocytes, based on forward and side scatter, then live cells, $B220^+$:$CD43^-$ cells, and then IgM^- cells, which were collected as the pre-B cell population. Cells were sorted on a BD FACSAria Fusion Flow cytometer.

Statistical Analyses

Statistical analyses were completed with Prism 9.

Results

Nemo deletion abrogates ATM-signaled gene expression changes in response to RAG DSBs induced during *Igk* recombination.

We use an established *ex vivo* primary mouse pre-B cell culture system to study ATM signals that regulate gene expression in response to RAG DSBs generated during *Igk* recombination. We culture total bone marrow cells from mice with inactivation of *Rag1* or the *Artemis* NHEJ gene along with transgenic expression of an IgH protein that signals pre-B cell differentiation and the BCL2 protein that suppresses apoptosis from un-repaired RAG DSBs (33, 39). The culture of *BCL2:IgH:Rag1*$^{-/-}$ (*BIR1*) and *BCL2:IgH:Artemis*$^{-/-}$ (*BIA*) bone marrow cells with IL7 cytokine leads to proliferation and expansion of pre-B cells in which *Rag1/2* transcription, *Igk* accessibility, and *Igk* recombination are suppressed (19, 33, 39, 40). Following withdrawal from IL7, *BIR1* and *BIA* cells arrest in G1 and transcriptionally upregulate *Rag1/2* expression and *Igk* accessibility (33, 39, 40). As *BIR1* cells express a disrupted *Rag1* gene that cannot produce Rag1 protein (47), they cannot

initiate *Igk* recombination; whereas, *BIA* cells initiate *Igk* recombination but cannot repair coding ends, leading to robust ATM signals from these RAG DSBs (33, 39). Accordingly, comparing IL7 withdrawn *BIR1* and *BIA* pre-B cells allows analysis of RAG DSB-induced, ATM-signaled changes in gene expression.

We sought to use this *ex vivo* primary mouse pre-B cell culture system to determine whether Nemo function is required for ATM-mediated signals that transiently feedback inhibit *Igk* recombination, *Rag1/2* expression, and J_k accessibility in response to RAG DSBs. We chose to inactivate Nemo because it is a central regulator of NFκB signaling and it was shown to be required for canonical NFκB factor activation in response to RAG DSBs using an inhibitory Nemo peptide in transformed pre-B cell lines (38). Thus, we postulated that Nemo would be required for ATM-mediated, NFκB-dependent gene expression changes induced by RAG DSBs. To test this, we inactivated Nemo in our *ex vivo* culture system using the *Mb1Cre* and $Nemo^{flox}$ alleles to disrupt Nemo expression in B lineage cells starting at the earliest stage of B cell development because germline *Nemo* deletion in mice is lethal (48). Mice with *Mb1Cre*-mediated deletion of *Nemo* exhibit normal B cell development through the immature B cell stage and only slight reductions in the numbers of more mature B cells (49). Through breeding, we established *BIR1* and *BIA* mice with a single *Mb1Cre* allele and homozygous $Nemo^{flox}$ alleles, referred to as $BIR1{:}Nemo^{-/-}$ and $BIA{:}Nemo^{-/-}$ mice, respectively. We also generated *BIR1* and *BIA* mice with homozygous $Nemo^{flox}$ alleles, but not *Mb1Cre*, referring to these as *BIR1* and *BIA* mice. To validate this experimental approach, we first used qRT-PCR to verify that Nemo mRNA was absent in $BIR1{:}Nemo^{-/-}$ and $BIA{:}Nemo^{-/-}$ pre-B cells cultured from bone marrow (Fig. 1 A). To confirm that *Nemo* deletion abrogates RAG DSB-induced, ATM-signaled changes in gene expression, we used qRT-PCR to quantify mRNAs encoding the pro-survival Pim2 kinase and the non-canonical NFκB2 factor because RAG DSB-signaled expression of these genes was disrupted by deletion of ATM and overexpression of a dominant negative IκBα protein, which represses NFκB signaling, in transformed pre-B cell lines (38). We detected higher levels of *Pim2* and *Nfkb2* transcripts in *BIA* cells relative to *BIR1* cells when each is cultured with IL7, and increased levels of both transcripts after removal of IL7 from *BIA* cells, but not from *BIR1* cells (Fig. 1 B, C), reflecting RAG DSB-signaled upregulation of these two genes. We found similar levels of *Pim2* and *Nfkb2* transcripts in *BIR1* and $BIR1{:}Nemo^{-/-}$ cells cultured with IL7 or removed from IL7 (Fig. 1 B, C), indicating that Nemo inactivation does not appreciably alter the basal expression of these genes in pre-B cells. In contrast, we observed no induction of *Pim2* and *Nfkb2* mRNA in $BIA{:}Nemo^{-/-}$ cells withdrawn from IL7 (Fig. 1 B, C), indicating that Nemo is necessary for RAG DSB-induced upregulation of *Pim2* and *Nfkb2* expression in pre-B cells. These data corroborate results from transformed pre-B cell lines that RAG DSBs induced during *Igk* recombination trigger gene expression changes through activation of canonical NFκB transcription factors (38). To confirm that not all gene expression changes in response to IL7 withdrawal are affected by Nemo deficiency, we used qRT-PCR to quantify mRNAs encoding *c-Myc* and *Metrn*, two genes that were identified as IL7-dependent but RAG DSB-independent through gene expression profiling and microarray analysis of primary pre-B cultures (40). Although we observed some minor differences of *c-Myc* or *Metrn* transcript levels between some genotypes in the presence of IL7 or 48 hours after removal from IL7, we detected similar reduction of transcript levels

for each gene among cells of all four genotypes following IL7 withdrawal (Fig. 1 D, E). These data indicate that Nemo inactivation has no profound effect on global gene expression in primary pre-B cells, thereby validating our experimental approach of using conditional deletion of Nemo to study responses to RAG cleavage of *Igk* loci in IL7 cultured pre-B cells.

For increased rigor, we assessed possibilities that the lack of *Pim2* and *Nfkb2* induction in *BIA:Nemo*$^{-/-}$ pre-B cells upon IL7 withdrawal might be due to impaired cell cycle dynamics or cellular survival in the absence of Artemis and Nemo protein. Encompassing all experiments, we found similar frequencies of small or large live pre-B cells, defined as B220^{+}, CD43^{-}, and IgM^{-} cells by flow cytometry, among cells of all four genotypes when cultured with IL7 or removed from IL7 (Fig. S1), revealing no discernable effects of combined Artemis and Nemo inactivation on cell cycle dynamics. To verify survival of cells with RAG DSBs was not impaired in the absence of Nemo, we analyzed the distribution of live, early apoptotic, late apoptotic, and necrotic large and small pre-B cells through Annexin V and propidium iodide staining and flow cytometry in *BIA* and *BIA:Nemo*$^{-/-}$ cells. We found a similar distribution of each of these populations among cultures of both genotypes, both in the presence of IL7 and after IL7 removal (Fig. S2) indicating no detectable increase in cell death from combined loss of Artemis and Nemo. This was expected as expression of the anti-apoptotic BCL2 protein would counter any impaired survival caused by the inability of *BIA:Nemo*$^{-/-}$ cells to upregulate expression of the pro-survival Pim2 protein.

Collectively, the above data validate our approach of using conditional Nemo inactivation and primary pre-B cell cultures to elucidate whether Nemo is required for RAG DSB-induced, ATM-signaled transient feedback inhibition of *Igk* recombination and transcriptional repression of both *Rag1* and *Rag2* expression and J_k accessibility.

Nemo is required for SpiC-dependent repression of J_k accessibility.

RAG DSBs induced during *Igk* recombination in pre-B cells signal feedback inhibition of J_k accessibility through expression of the SpiC transcriptional repressor, which displaces the PU.1 transcriptional activator from the 3’ *Igk* enhancer in response to RAG DSBs (40). This signaling pathway involves ATM-dependent upregulation of the *Nfbk2* and *Relb* non-canonical NFκB factors and proteolysis of NFκB2 (p100) into p52 (40), consistent with p52 partnering with RelB to transcriptionally induce *Spic* expression. Considering that Nemo inactivation abolishes RAG DSB-triggered upregulation of *Nfbk2* transcripts (Fig. 1 F), we sought to confirm that Nemo is necessary for RAG DSBs to induce SpiC expression. We employed qRT-PCR to measure *Spic* mRNA in *BIR1*, *BIR1:Nemo*$^{-/-}$, *BIA*, and *BIA:Nemo*$^{-/-}$ cells before and after IL7 withdrawal using the samples for which we assayed *Nfbk2* transcripts (Fig. 1). We detected *Spic* transcripts only in *BIA* cells, and interestingly at similar levels before and at all times after IL7 removal (Fig. 1 F). This analysis, which was not presented by Bednarski *et al.*, reveals that the low levels of RAG DSBs in Artemis-deficient pre-B cells cultured in IL7 trigger full upregulation of *Spic* expression. Presumably, the small increase of *Nfkb2* transcripts from the few RAG DSBs induced in IL7 cultured cells is sufficient to promote maximal SpiC expression. The absence of *Spic* transcripts in *BIR1* cells (Fig. 1 F) is consistent with results from Bednarski *et*

al. showing that RAG DSBs activate SpiC protein expression in pre-B cells. The absence of *Spic* transcripts in *BIA:Nemo*$^{-/-}$ cells (Fig. 1 F) indicates that Nemo is required for RAG DSBs induced during *Igk* recombination to signal non-canonical NFκB factor-directed transcriptional activation of SpiC expression. Accordingly, Nemo enables RAG DSB-triggered, ATM-signaled feedback inhibition of J_k accessibility. To determine whether Nemo might effect accessibility of J_k gene segments before RAG cleavage, we used qPCR to quantify germline J_k transcripts (*Jktrx*) in *BIR1* and *BIR1:Nemo*$^{-/-}$ cells as accessible segments would not be cleaved in these samples. We observed that *BIR1:Nemo*$^{-/-}$ cells expressed slightly lower levels of *Jktrx* at all time points compared to *BIR1* cells, yet these differences did not reach statistical significance (Fig. 1 G). Therefore, we conclude that Nemo has a negligible role in promoting accessibility of J_k gene segments before RAG cleavage.

Nemo is required for ATM-signaled feedback inhibition of *Igk* recombination.

We previously elucidated that ATM signals coordinate initiation of *Igk* rearrangements between alleles by using Southern blots to quantify RAG cleavage of J_k segments in *BIA* pre-B cells incapable of repairing *Igk* coding ends (33). We used this same approach to determine whether Nemo is required for RAG DSBs induced during *Igk* recombination on one allele to signal ATM-dependent feedback inhibition of *Igk* recombination on the other allele. When cultured with IL7, most *BIA* pre-B cells maintain *Igk* loci in germline (GL) configuration (Fig. 2 A–C) because IL7 represses RAG expression and *Igk* accessibility (19, 33, 39). Removal of IL7 leads to initiation of *Igk* recombination with cells losing GL loci and accumulating *Igk* coding ends (CEs) (Fig. 2 A–C), which cannot be processed into coding joins due to the absence of Artemis (33, 39). By 48 hours of IL7 withdrawal from *BIA* cells, roughly half the *Igk* alleles remain GL and half accumulate CEs, whereas chemical inhibition of ATM kinase activity leads to near complete loss of GL alleles (Fig. 2 A–C). As before (33), these data show that RAG DSBs induced during *Igk* recombination on one allele signal via ATM to suppress RAG cleavage of the other *Igk* allele. To determine if this ATM-signaled inter-allelic control of *Igk* recombination is Nemo dependent, we quantified RAG cleavage of *Igk* alleles in IL7 withdrawn *BIA:Nemo*$^{-/-}$ pre-B cell cultures. We performed this analysis in the presence and absence of an ATM kinase inhibitor as a positive control for inactivation of ATM-signaled inter-allelic control of *Igk* recombination. At 48 and 72 hours after IL7 withdrawal from *BIA:Nemo*$^{-/-}$ cells, we observed nearly complete loss of GL alleles regardless of the absence or presence of ATM inhibitor (Fig. 2 A–C). These data indicate that Nemo expression is necessary for RAG DSBs induced during *Igk* recombination on one allele to signal ATM-mediated feedback inhibition of RAG cleavage on the other *Igk* allele.

For more rigorous and comprehensive analyses, we developed a Taqman assay to quantify RAG cleavage at each of the four functional J_k gene segments (*Jk1*, *Jk2*, *Jk4*, and *Jk5*) (Fig. 2 D). Using primers that anneal to sequences surrounding each J_k RSS, we can detect RAG cleavage at individual J_k segments by loss of the amplification signal (Fig. 2 D); accordingly, a decrease in signal correlates with an increase in cleavage. To validate this assay, we quantified RAG cleavage by Taqman in the same samples assayed by Southern blot (Fig. 2 B, C). The Taqman data reflect the Southern blot data in that after 48 hours

of IL7 withdrawal, cells with inactivation of ATM and/or Nemo show increased cleavage of each J_k segment compared to *BIA* cells that were ATM and/or Nemo sufficient (Fig. 2 E; Fig. S3 A). An advantage of the Taqman assay is that it requires far less cells for analysis. Thus, we were able to quantify RAG cleavage of individual J_k gene segments in the same pre-B cell samples that we analyzed gene expression (Fig. 1). We detected no RAG cleavage of any J_k segments in Rag1-deficient *BIR1* or *BIR1:Nemo*$^{-/-}$ cells (Fig. 2 F; Fig. S3 B). In Artemis-deficient *BIA* and *BIA:Nemo*$^{-/-}$ cells, we detected increasing levels of RAG cleavage at each J_k segment over time following IL7 withdrawal (Fig. 2 F; Fig. S3 B). Notably, at 48 and 72 hours after IL7 withdrawal, the levels of cleavage at each J_k segment was greater in *BIA:Nemo*$^{-/-}$ cells as compared to *BIA* cells (Fig. 2 F; Fig. S3 B), indicating that Nemo is required to limit induction of RAG DSBs at *Igk* loci. Combined with the quantification of gene expression, these data offer direct evidence that RAG DSBs induced at J_k segments during *Igk* recombination trigger Nemo-dependent upregulation of *Pim2* and *Nfkb2* transcripts.

Nemo is required for complete RAG DSB-induced repression of *Rag1* and *Rag2* transcription.

DSBs induced by RAG or genotoxic agents, including irradiation or small molecules, signal through ATM to suppress *Rag1* and *Rag2* transcript levels (33, 45, 50), where at least genotoxic DSBs do so by repressing *Rag1* and *Rag2* transcription rather than stimulating turnover of *Rag1* and *Rag2* transcripts (45). Therefore, we sought to determine whether RAG DSBs generated during *Igk* recombination also transcriptionally repress *Rag1* and *Rag2* expression. For this purpose, we used Click-iT technology to measure levels of nascent *Rag1* and *Rag2* transcripts in *BIR1* and *BIA* pre-B cell cultures in the presence or absence of IL7. The Click-iT approach uses incorporation of ethylene uridine (EU) into RNAs during transcription to label transcripts, which are then conjugated with biotin, collected by streptavidin beads, and quantified by qRT-PCR. Notably, we are able to assay *Rag1* transcripts in *Rag1*$^{-/-}$ cells because the Neomycin-resistance gene that inactivates *Rag1* disrupts the second exon, leaving intact the promoter and first exon junction (47). To measure nascent transcripts, we incubated cells with EU for an hour prior to collecting cells in IL7 or at each time point after IL7 withdrawal. By comparing levels of EU-labelled transcripts in *BIR1* cells without RAG DSBs to *BIA* cells with un-repaired RAG DSBs, we can quantify the effect of RAG DSBs on transcription of *Rag1*, *Rag2*, and the *Wasp* gene that is not regulated by DSBs. The amounts of EU-labelled *Wasp* transcripts were equivalent in *BIR1* and *BIA* cells at each time point, revealing that RAG DSBs do not alter *Wasp* transcription (Fig. 3 A). In contrast, at each time point, we detected lower levels of EU-labelled *Rag1* and *Rag2* transcripts in *BIA* cells relative to *BIR1* cells (Fig. 3 A), indicating that RAG DSBs induced during *Igk* recombination in pre-B cells suppress *Rag1* and *Rag2* transcription. Notably, in both *BIA* and *BIR1* cells, IL7 withdrawal lead to increased levels of EU-labelled *Rag1* and *Rag2* transcripts at early time points, a peak at 48 hours for *Rag1* or 24 hours for *Rag2*, and lower than peak levels at later time points (Fig. 3 A). These data reveal that IL7 removal from *BIR1* cells without RAG DSBs leads to distinct kinetics of activation and rates of sustained transcription over time for *Rag1* and *Rag2*. These data also show that IL7 withdrawal from *BIA* cells leads to initial activation of *Rag1* and *Rag2* transcription, while accumulation of RAG DSBs triggers downregulation

of *Rag1* and *Rag2* transcription beyond IL7-dependent changes over time. Therefore, we conclude that RAG DSBs generated during *Igk* recombination transcriptionally repress *Rag1* and *Rag2* expression.

We next sought to ascertain if RAG DSBs generated during *Igk* recombination in pre-B cells use Nemo-dependent mechanisms to transcriptionally downregulate *Rag1* and *Rag2* expression. For this purpose, we initially quantified steady state levels of *Rag1* and *Rag2* transcripts in *BIR1*, *BIR1:Nemo*$^{-/-}$, *BIA*, or *BIA:Nemo*$^{-/-}$ pre-B cell cultures before and after IL7 withdrawal. At each time point assayed, we detected no differences in levels of *Rag1* or *Rag2* transcripts between *BIR1* and *BIR1:Nemo*$^{-/-}$ cells (Fig. 3 B), indicating that Nemo inactivation does not alter steady state levels of *Rag1* or *Rag2* transcripts in pre-B cells unable to generate RAG DSBs. Therefore, our data confirm that the stimulation of *Rag1* and *Rag2* transcription after IL7 withdrawal and G1 arrest of pre-B cells does not require Nemo expression. At each time point after IL7 removal, we observed lower levels of steady state *Rag1* and *Rag2* transcripts in *BIA* cells as compared to *BIR1* cells (Fig. 3 B), reflecting that RAG DSBs induced during *Igk* recombination repress *Rag1* and *Rag2* transcription. Notably, for each time point after IL7 withdrawal, the steady state levels of *Rag1* and *Rag2* transcripts were higher in *BIA:Nemo*$^{-/-}$ cells versus *BIA* cells (Fig. 3 B), indicating that Nemo is required for RAG DSBs to fully repress *Rag1* and *Rag2* expression. To more quantitatively illustrate this, we calculated the fold change in levels of *Rag1* and *Rag2* transcripts between *BIA* and *BIR1* cells that express or lack Nemo (Fig. 3 C). As values below 1 represent lower expression in the presence of RAG DSBs, these data demonstrate definitively that RAG DSBs induced during *Igk* recombination repress *Rag1* and *Rag2* expression when Nemo is present, but to lesser extents when Nemo is absent (Fig. 3 C). Finally, to determine whether Nemo contributes to RAG DSB triggered repression of *Rag1* and *Rag2* transcription, we used Click-iT technology to measure nascent transcripts in *BIA* and *BIA:Nemo*$^{-/-}$ pre-B cells before and after IL7 withdrawal. At all times, we found that nascent transcripts of *Rag1* and *Rag2*, but not *Wasp*, were higher in *BIA:Nemo*$^{-/-}$ cells compared to *BIA* cells (Fig. 3 D), indicating that Nemo is necessary for RAG DSBs to completely suppress *Rag1* and *Rag2* transcription. These data demonstrate that RAG DSBs induced during *Igk* recombination in pre-B cells activate Nemo-dependent signals to transcriptionally downregulate *Rag1* and *Rag2* expression.

Considering that Nemo inactivation disrupts RAG DSB-induced repression of *Rag1/Rag2* and induction of *Spic*, whose protein product represses J_k accessibility, we sought to determine i) the contribution of the role of SpiC alone in suppressing bi-allelic *Igk* recombination when RAG expression is maintained, and ii) the potential role of SpiC in DSB-induced *Rag1* and *Rag2* repression. For this purpose, we attempted to quantify RAG cleavage of J_k gene segments and *Rag1* and *Rag2* transcripts in *BIA* pre-B cells on a *Spic*-deficient background. However, we were unable to accomplish this analysis because *BIA:Spic*$^{-/-}$ mice were born at sub-Mendelian frequencies and those born were unhealthy and died within a few days. Thus, we proceeded to ascertain whether the SpiC transcriptional repressor is responsible for reducing *Rag1* and *Rag2* transcription in response to DSBs induced by etoposide. To this aim, we treated total bone marrow from wild-type (*WT*), *Spic*$^{-/-}$, and *Mb1Cre*$^{+}$*:Nemo*$^{flox/flox}$ mice with etoposide for 1 or 4 hours before isolating mRNA and using qRT-PCR to quantify *Rag1* and *Rag2* transcripts. In all

genotypes, we observed increased transcripts of the DSB responsive *p21* gene at both time points (Fig. 4 A), validating that the etoposide treatment induced DSBs. We detected lower levels of *Rag1* and *Rag2* transcripts at both time points in *WT* and *Spic*$^{-/-}$ cells, but no change in the amounts of these transcripts in *Mb1Cre*$^{+}$*:Nemo*$^{flox/flox}$ (*Nemo*$^{-/-}$) cells (Fig. 4 B, C). These data show that inactivation of the SpiC transcriptional repressor has no obvious effect on genotoxic DSB-induced repression of *Rag1* and *Rag2* expression. As transcriptional changes studied thus far have been consistent between DSBs induced in pre-B cells by RAG or genotoxic agents, this finding provides strong support for the notion that RAG DSBs induced during *Igk* recombination in *Spic*-deficient pre-B cells feedback inhibit RAG expression but not J_k accessibility.

Nemo is dispensable for efficient repair of RAG DSBs unlike ATM.

We have shown that conditional *Nemo* deletion provides a means to inactivate ATM signals that suppress RAG expression and J_k accessibility. Although to our knowledge Nemo has not been implicated in DSB repair, we thought that it was critical to confirm (or not) that Nemo deficiency does not impair the repair of RAG DSBs like ATM inactivation, for example by impairing the expression of ATM substrates. ATM stabilizes RAG post-cleavage complexes to maintain coding ends and signal ends close together and promote formation of coding joins and signal joins (34, 51). A hallmark of ATM deficiency is an increased incidence of attempted inversional V(D)J rearrangements aberrantly resolving as deletional hybrid joins from ligation of a coding end and a signal end following the escape of intervening DNA (34) (Fig. 5 A). Thus, to rule out a role for Nemo in DSB repair, we measured hybrid joins resulting from attempted inversional V_k-to-J_k rearrangements. For this purpose, we designed and employed a Taqman assay to quantify hybrid joins formed during attempted inversional V_k-to-J_k1 rearrangements for four different V_k gene segments (Fig. 5 A), which we performed on genomic DNA of pre-B cells sorted from the bone marrow of *WT, Atm*$^{-/-}$*, or Mb1Cre*$^{+}$*:Nemo*$^{flox/flox}$ mice. As compared to *WT* cells, we observed higher levels of V_k/J_k1 hybrid joins for each of the V_k segments in *Atm*$^{-/-}$ cells (Fig. 5 B), reflecting decreased stability of RAG post-cleavage complexes in the absence of ATM. In contrast, we detected normal levels of V_k/J_k1 hybrid joins for each of the V_k segments in *Mb1Cre*$^{+}$*:Nemo*$^{flox/flox}$ cells (Fig. 5 B), demonstrating that Nemo deficiency does not cause a defect in DSB repair like ATM deficiency. Thus, conditional Nemo inactivation in developing B cells indeed inactivates ATM signaling functions that suppress RAG expression and J_k accessibility while leaving ATM functions in DSB repair intact. In this context, the *Mb1Cre*$^{+}$*:Nemo*$^{flox/flox}$ background provides an experimental approach to assess whether RAG DSB-induced, ATM-signaled feedback inhibition of *Igk* recombination has a role in enforcing Igκ allelic exclusion independent of ATM-mediated DSB repair.

Nemo-dependent, ATM-signaled transient feedback inhibition of *Igk* recombination enforces Igκ allelic exclusion.

To determine whether Nemo-dependent, ATM-signaled feedback inhibition of bi-allelic initiation of *Igk* recombination enforces Igκ allelic exclusion, we made and assayed *Mb1Cre*$^{+}$*:Nemo*$^{flox/flox}$ mice with one *Igk* allele carrying mouse C_k constant region exon replaced with human sequences. This C_k mouse/human heterozygous (Ck$^{m/h}$) background provides an allotypic marker that enables analysis of Igκ expression from each allele

using anti-Cκ^m and anti-Cκ^h antibodies (52). We previously used this approach to show that ATM helps enforce Igκ allelic exclusion (33). In this study, we observed higher frequencies of bone marrow and splenic B cells with bi-allelic Igκ expression in *Mb1Cre*$^+$*:Nemo*$^{flox/flox}$*Igk*$^{m/h}$ mice as compared to control *Nemo*$^{flox/flox}$*Igk*$^{m/h}$ and *Mb1Cre*$^+$*:Igk*$^{m/h}$ mice (Fig. 6 A, B; Fig. S3 C, D). The frequencies of splenic B cells expressing similar high levels of surface Igκ^m and Igκ^h were 1.6-fold greater in *Mb1Cre*$^+$*:Nemo*$^{flox/flox}$*Igk*$^{m/h}$ mice (Fig. 6 B; Fig. S3 C, D), indicating that Nemo inactivation impairs the enforcement of Igκ allelic exclusion. These data show that Nemo-dependent signals help establish Igκ allelic exclusion. The critical signals could include those that transcriptionally down-regulate RAG expression, J_k accessibility, or both. To investigate this further, we generated and analyzed *Spic*$^{-/-}$*Igk*$^{m/h}$ mice as inactivation of SpiC disrupts DSB-induced down-regulation of J_k accessibility but not RAG expression. We found that the frequencies of B cells with bi-allelic Igκ expression were equivalent between *Spic*$^{-/-}$*Igk*$^{m/h}$ mice and *Igk*$^{m/h}$ mice (Fig. 6 A, B), revealing that disruption of SpiC-mediated repression of J_k accessibility alone is not sufficient to impair Igκ allelic exclusion. Accordingly, our data presented in this study collectively illuminate a critical role for Nemo-dependent, ATM-signaled transcriptional repression of RAG expression in establishing Igκ allelic exclusion.

Discussion

Our study demonstrates that Nemo-dependent, ATM-mediated signals from RAG DSBs generated during V_k-to-J_k recombination feedback inhibit RAG cleavage to enforce Igκ allelic exclusion. Although prior studies showed that ATM helps enforce Igκ, IgH, and TCRβ allelic exclusion, these analyses could not distinguish contributions of ATM in promoting coding join formation versus signaling DSB-initiated transient feedback inhibition of recombination (33, 37). In our study, we employed Artemis-deficient primary pre-B cells that allow analyses of RAG DSB signaling independent of coding join formation to determine that Nemo inactivation hinders RAG DSBs from signaling feedback inhibition of initiation of *Igk* recombination and allows for an increase of RAG DSBs at *Igk* loci. We also showed that inactivation of Nemo in developing mouse B cells does not impair *Igk* coding join formation as does ATM deficiency, yet still results in increased frequency of mature B cells that express Igκ proteins from both alleles similar to ATM inactivation. While we show that *Mb1Cre*$^+$*:Nemo*$^{lox/flox}$*Igk*$^{m/h}$ mice develop 1.6-fold higher than normal frequencies of B cells with bi-allelic Igκ expression, our lab previously reported that *Mb1Cre*$^+$*:Atm*$^{flox/flox}$*Igk*$^{m/h}$ mice develop ~2.5-fold greater than normal frequencies of such cells (33). Due to institutional research restrictions prompted by the Covid19 pandemic, we were not able to conduct direct side-by-side comparisons of *Mb1Cre*$^+$*:Nemo*$^{flox/flox}$*Igk*$^{m/h}$ and *Mb1Cre*$^+$*:Atm*$^{flox/flox}$*Igk*$^{m/h}$ mice. Therefore, we cannot distinguish between a *bona fide* greater degree of bi-allelic Igκ expression from inactivation of ATM versus variables inherent in comparing studies performed by different people several years apart. We also note that in this study, we quantified dual-Igκ^+ cells regardless of Igκ^m and Igκ^h expression levels, while in our prior study, we only included cells expressing Igκ^m and Igκ^h at equivalently high levels. Nevertheless, our data here indicate that ATM helps enforce Igκ allelic exclusion, at least in part, via Nemo-dependent signals that transiently

suppress RAG cleavage of *Igk* gene segments. Our current work also shows that Nemo deficiency blocks RAG DSBs induced during V_k-to-J_k recombination from signaling ATM-dependent transcriptional downregulation of *Rag1/Rag2* and transcriptional activation of *Spic*. Although SpiC suppresses accessibility and RAG cleavage of J_k gene segments (40), we found that SpiC deficiency neither prevented DSB-signaled repression of *Rag1* and *Rag2* transcripts nor elevated the incidence of B cells with bi-allelic Igκ protein expression. These findings argue that disruption of SpiC-mediated transcriptional repression of J_k accessibility in response to RAG DSBs without disrupting transcriptional repression of *Rag1* and *Rag2* is not sufficient to disrupt Igκ allelic exclusion. Consequently, we propose that Nemo-dependent down-regulation of RAG expression is a dominant mechanism by which ATM signals transient feedback inhibition of *Igk* recombination and thereby helps implement Igκ allelic exclusion.

The modest increase in the frequency of B cells with bi-allelic Igκ protein expression from inactivation of Nemo most likely reflects that RAG DSB-activated transient feedback inhibition of *Igk* recombination cooperates with mono-allelic initiation and BCR-signaled permanent feedback inhibition of V_k-to-J_k recombination to achieve Igκ allelic exclusion. The assembly of *Igk* genes requires accessibility of at least one V_k and J_k gene segment, RAG binding to the RSS one of these segments, and alteration of *Igk* locus topology to place V_k and J_k segments in physical proximity to allow RAG-mediated synapsis, cleavage, and joining. Asynchronous replication timing of individual *Igk* alleles is clonally and permanently established in progenitor B cells (28). The J_k segments of early replicating alleles become preferentially accessible and recombined in primary pre-B cells (28, 29), implying that asynchronous replication underlies an epigenetic mechanism for establishing mono-allelic initiation of *Igk* recombination. A study using pre-B cell lines revealed transcription and chromatin accessibility of only a limited number of V_k gene segments on each allele (30). However, another study revealed that primary pre-B cells harbor mono-allelic transcripts from a large number of contiguous V_k gene segments positioned in transcription factories, with different sets of V_k segments positioned and transcribed among individual cells (31). Each of these findings are consistent with a model wherein only transcribed V_k segments would be available for synapsis with J_k gene segments to facilitate rearrangement (22), providing another potential epigenetic mechanism for the mono-allelic initiation of *Igk* recombination. Our data that Nemo and ATM each blocks RAG cleavage of J_k segments on both alleles in G1-arrested, NHEJ-deficient primary pre-B cells incapable of assembling and expressing *Igk* genes demonstrates that DSB-induced feedback inhibition helps prevent bi-allelic initiation of *Igk* recombination. This finding also shows that formation of a VJ_k coding join on the first recombining allele is not required for initiation of recombination on the other allele. Our data supports a model wherein the transient transcriptional downregulation of RAG expression signaled from *Igk* recombination on one allele allows more time for the resulting VJ_k coding join to be generated, expressed, and undergo selection before initiation of *Igk* rearrangement on the other allele. This response might function either constitutively during all V_k-to-J_k rearrangements or only as an SOS-like response for a subset of recombination events where RAG-generated coding ends are not immediately repaired. If this first VJ_k coding join is repaired out-of-frame, the attenuation of DSB signaling will re-establish RAG expression and permit *Igk*

recombination on either allele. This cycle could continue until formation of an in-frame VJ_k coding join or exhaustion of all possible *Igk* rearrangements. If a VJ_k coding join is in-frame and the resulting receptor positively selected, BCR signals will drive differentiation to the mature B cell stage and signal permanent feedback inhibition of *Igk* recombination, at least in part through transcriptional silencing of RAG expression. Alternatively, if an in-frame VJ_k coding join generates an autoreactive receptor, resulting strong BCR signals will halt developmental progression at the immature B cell stage and transcriptionally up-regulate RAG expression to promote receptor editing through additional V_k-to-J_k rearrangements. Receptor editing can occur on either allele (25); however, to our knowledge, it has not been reported whether epigenetic mechanisms might direct mono-allelic initiation of *Igk* recombination during this process. We have not investigated if RAG DSBs generated during receptor editing signal transient feedback inhibition of *Igk* recombination to limit V_k-to-J_k rearrangements to one allele. Developing αβ T cells exhibit developmental-stage specific repression of RAG expression in response to DSBs, with this response present in pro-T cells that assemble *Tcrb*, *Tcrd*, and *Tcrg* genes, but not in pre-T cells that assemble *Tcra* genes (45). Accordingly, additional studies are warranted to determine whether the RAG DSB-induced transient feedback inhibition of *Igk* recombination that we observe in pre-B cells also operates during receptor editing in immature B cells.

Our study establishes that RAG DSBs generated during *Igk* recombination in primary pre-B cells signal via Nemo-dependent, ATM-mediated mechanisms to transcriptionally repress *Rag1* and *Rag2* expression, suppress further RAG cleavage of J_k gene segments, and enforce Igκ allelic exclusion. We did not assay Rag1 or Rag2 protein in this study. However, prior work from our lab has shown that the increased levels of *Rag1* and *Rag2* transcripts in pre-B cells due to ATM inactivation correlates with a higher level of Rag1 protein, but not Rag2 protein (33), and that genotoxic DSBs induced in pre-B cells repress levels of *Rag1* and *Rag2* transcripts and Rag1 protein, but not Rag2 protein, which we discovered has a half-life of at least 12 hours in G1-arrested transformed pre-B cells (45). As RAG DSBs accumulate at J_k segments for up to 48 hours after IL7 withdrawal of primary *BIA* pre-B cells (33, 39, 40), it is not possible to determine how fast Rag1 protein is downregulated following initiation of *Igk* recombination on one allele. The synchronous induction of DSBs in many primary pre-B cells by ionizing radiation signals a 50% reduction of Rag1 protein levels within an hour and complete loss by four hours (45). We consider it likely that RAG DSBs induced during *Igk* recombination signal downregulation of Rag1 protein, and thereby RAG endonuclease activity, with similar kinetics and extent. Nevertheless, the persistence of *Rag1* and *Rag2* transcription and corresponding bi-allelic RAG cleavage of J_k segments in *BIA:Nemo*$^{-/-}$ primary pre-B cells indicates that Nemo-dependent transcriptional downregulation of RAG expression is critical for DSB-induced feedback inhibition of RAG endonuclease activity. Previous observations by our lab and others in transformed pre-B cell lines have led to speculation that ATM-dependent phosphorylation of conserved sites on Rag1 and/or Rag2 protein might repress RAG endonuclease activity and thereby help enforce allelic exclusion (53, 54). The induction of genotoxic DSBs in pre-B cell lines also triggers ATM-mediated nuclear-to-cytoplasmic export of Rag2 protein that is blocked by mutation of Rag2 threonine 490 to a non-phosphorylatable amino acid (55). In primary pre-B cells, the Rag1 amino terminus regulates nucleolar sequestration of

Rag1 protein, which lowers V(D)J recombination activity (56). Considering that the Rag1 amino terminus has conserved consensus sites for ATM-dependent phosphorylation, it is conceivable that RAG DSBs trigger the retention of Rag1 at nucleoli to mediate feedback inhibition of *Igk* recombination before downregulation of Rag1 protein. Our analyses of Nemo-deficient primary B lineage cells demonstrates that any potentially relevant ATM-mediated post-translational inhibition of RAG endonuclease activity is not sufficient to mediate DSB-induced feedback inhibition of *Igk* recombination and resulting Igκ allelic exclusion. However, the elucidation and specific inactivation of mechanisms by which Nemo orchestrates DSB-signaled transcriptional repression of *Rag1* and *Rag2* transcripts are required to determine whether Nemo-independent, ATM-dependent post-translational mechanisms contribute to inter-allelic regulation of *Igk* gene recombination and expression. Theoretically, beyond suppressing RAG endonuclease activity, such potential mechanisms could downregulate accessibility of V_k gene segments and/or antagonize the dynamic compaction of *Igk* loci.

Our data demonstrating that Nemo deficiency disrupts RAG DSB-induced, ATM-mediated transcriptional downregulation of RAG expression implies that NFκB factors act on the *Rag1/Rag2* locus to mediate this response. Studies in immortalized cell lines have elucidated signaling pathways through which DSBs drive nuclear pools of Nemo and ATM into the cytoplasm to generate or activate IKK complexes, respectively, which stimulate nuclear accumulation of canonical NFκB factors (57–59). As Nemo inactivation prevents stimulus-induced activation of canonical NFκB factors (42–44), any of these proteins (RelA, NFκB1, and c-Rel) could mediate RAG DSB-signaled repression of *Rag1/Rag2* transcription. Experiments in pre-B cell lines have demonstrated that RAG DSBs trigger ATM-dependent proteolysis of the non-canonical NFκB2 protein into the p52 form that enters the nucleus to regulate gene expression (40). Considering our data that Nemo inactivation impairs DSB-signaled, NFκB2-mediated induction of *Spic* transcripts, NFκB2 and its non-canonical NFκB partner RelB also might suppress *Rag1/Rag2* transcription upon RAG cleavage of J_k segments. Although NFκB-mediated activation of gene expression has been researched extensively, how NFκB proteins inhibit gene transcription remains under investigated. One study using a non-lymphoid cell line showed that DSBs trigger ATM phosphorylation of RelA, which recruits histone deacetylase 1 to repress expression of genes whose transcription RelA promotes (60). This mechanism is unlikely involved in DSB-induced feedback inhibition as our finding that basal *Rag1/Rag2* transcription is unaffected by deficiency of Nemo argues against a role for RelA in stimulating *Rag1* and *Rag2* expression before initiation of *Igk* recombination. Lipopolysaccharide (LPS) treatment of a B lymphoma cell line triggers canonical NFκB factor-dependent repression of gene expression directed, at least in part, by *de novo* binding of RelA to sequences that overlap with AP1 binding sites within target loci (61). As this regulation almost certainly would require Nemo function, RelA is a plausible candidate NFκB factor for effecting RAG DSB-induced downregulation of *Rag1* and *Rag2* transcription. Nevertheless, to elucidate the precise Nemo-dependent mechanisms that repress *Rag1* and *Rag2* expression in pre-B cells, it will be necessary to identify what NFκB factors bind along the *Rag1/Rag2* locus, and where, upon initiation of *Igk* recombination. However, an alternative scenario must be considered where Nemo-dependent, NFκB activity drives expression of another

transcriptional repressor whose function at *Rag1/Rag2* depends on phosphorylation by ATM. Thus, agnostic approaches also should be pursued to elucidate the Nemo-dependent mechanisms of DSB-induced downregulation of *Rag1* and *Rag2* transcription. Determining and specifically inactivating these mechanisms is necessary to evaluate the contribution of Nemo-dependent, ATM-mediated repression of *Rag1* and *Rag2* expression in enforcing Igκ allelic exclusion.

The Gadd45α stress-regulated protein was previously implicated in the regulation of *Rag1/2* expression. After Gadd45α was shown to drive FOXO1-dependent expression of *Rag1/2* in an immortalized mouse pre-B cell line (62), we reported that Gadd45α expression correlated with *Rag1/2* expression and both increased in the absence of ATM following the induction of RAG DSBs in primary pre-B cells (33). From these data, we presented a model in which ATM repressed *Rag1/2* expression through downregulation of Gadd45α. However, additional work in our lab and the Guikema lab has not supported this model. The Guikema lab showed in multiple different Abelson transformed cell lines that DSBs induced by genotoxic drugs repressed *Rag1/2* expression but had no effect on Gadd45α expression (50). Furthermore, we demonstrated that i) the kinetics of *Gadd45α* downregulation is too slow to cause genotoxic DSB-induced transcriptional repression of *Rag1/2* in primary pre-B cells, and ii) ectopic *Gadd45α* over-expression does not interfere with DSB-induced repression of *Rag1/2* in an Abelson transformed pre-B cell line (45). Therefore, we concluded that repression of *Gadd45α* has no role in DSB-induced repression of *Rag1/2*. Nevertheless, to determine whether *Gadd45α* expression is impacted in Nemo-deficient primary pre-B cells, we assayed *Gadd45α* transcripts using qPCR in our pre-B cell culture samples. At each time point assayed, we detected no differences in *Gadd45α* transcripts between *BIR1* and *BIR1:Nemo*$^{-/-}$ cells (Fig. S3 E), indicating that Nemo inactivation does not alter steady state levels of *Gadd45α* transcripts in pre-B cells unable to generate RAG DSBs. Conversely, we found higher *Gadd45α* transcripts in *BIA:Nemo*$^{-/-}$ pre-B cells as compared to *BIA* pre-B cells (Fig. S3 E), indicating that Nemo inactivation increases *Gadd45α* expression in pre-B cells with persistant RAG DSBs. These data present another correlation between *Gadd45α* and *Rag1/2* expression and are consistent with a model wherein Nemo is simultaneously contributing to repression of both *Gadd45α* and *Rag1/2* transcripts, but where this downregulation of *Gadd45α* does not drive transcriptional repression of *Rag1/2* expression in response to RAG DSBs. As stated above, additional agnostic studies will be necessary to elucidate mechanisms governing Nemo-dependent, RAG DSB-induced repression of *Rag1/2* and the role of this response in Igκ allelic exclusion.

While our data validate that RAG DSB-induced feedback inhibition of V(D)J recombination contributes to Igκ allelic exclusion, it remains to be determined whether such signaling helps achieve mono-allelic assembly and expression of IgH and TCRβ genes. In this context, the diminished enforcement of IgH and TCRβ allelic exclusion in ATM-deficient mice could arise from impaired DSB signaling, repair, or both. As for pre-B cells, genotoxic DSBs induced in pro-B cells or pro-T cells trigger downregulation of *Rag1* and *Rag2* transcripts (45); yet, the potential role of ATM in signaling this response remains to be determined. Moreover, it has not been established whether RAG DSBs generated during the *D*-to-*J* and/or *V*-to-*DJ* rearrangement steps of IgH and TCRβ gene assembly signal ATM-mediated repression of *Rag1* and *Rag2* transcription and resulting downregulation of RAG expression.

The finding that genotoxic DSBs have no discernable effect on *Rag1* and *Rag2* transcript levels in pre-T cells revealed the existence of lymphocyte lineage- and developmental stage-specific DSB responses, at least pertaining to feedback inhibition of V(D)J recombination (45). Therefore, it is important to determine whether RAG DSBs induced during *D*-to-*J* or *V*-to-*DJ* recombination on one IgH or TCRβ allele transiently block initiation of V(D)J recombination on the second allele and, if so, elucidate the underling mechanisms and physiological roles for this inter-allelic regulation of antigen receptor gene assembly. The approaches that we have described here to study DSB-induced feedback inhibition of *Igk* recombination would facilitate such studies of IgH and TCRβ allelic exclusion.

Supplementary Material

Refer to Web version on PubMed Central for supplementary material.

Acknowledgements

We thank Erica Culberson and Morgann Klink for help with genotyping and Katharina Hayer for her guidance in statistical analyses. The authors have no competing financial interests to declare.

This work was supported by T32 GM-07229 (R.A.G.), F31AI152354 (R.A.G.), RO1 AI 112621 (C.H.B.), and RO1 AI 130231 (C.H.B.)

References

1. Schatz DG, and Swanson PC. 2011. V(D)J Recombination: Mechanisms of Initiation. Annu. Rev. Genet 45: 167–202. [PubMed: 21854230]
2. Zhao L, Frock RL, Du Z, Hu J, Chen L, Krangel MS, and Alt FW. 2016. Orientation-specific RAG activity in chromosomal loop domains contributes to Tcrd V(D)J recombination during T cell development. J. Exp. Med 213: 1921–1936. [PubMed: 27526713]
3. Chen L, Zhao L, Alt FW, and Krangel MS. 2016. An Ectopic CTCF Binding Element Inhibits Tcrd Rearrangement by Limiting Contact between Vδ and Dδ Gene Segments. J. Immunol 197: 3188–3197. [PubMed: 27613698]
4. Lin SG, Ba Z, Alt FW, and Zhang Y. 2018. RAG Chromatin Scanning During V(D)J Recombination and Chromatin Loop Extrusion are Related Processes. In Advances in Immunology, 1st ed. vol. 139. Elsevier Inc. 93–135. [PubMed: 30249335]
5. Jain S, Ba Z, Zhang Y, Dai H-Q, and Alt FW. 2018. CTCF-Binding Elements Mediate Accessibility of RAG Substrates During Chromatin Scanning. Cell 174: 102–116.e14. [PubMed: 29804837]
6. Zhang Y, Zhang X, Ba Z, Liang Z, Dring EW, Hu H, Lou J, Kyritsis N, Zurita J, Shamim MS, Presser Aiden A, Lieberman Aiden E, and Alt FW. 2019. The fundamental role of chromatin loop extrusion in physiological V(D)J recombination. Nature 573: 600–604. [PubMed: 31511698]
7. Hill L, Ebert A, Jaritz M, Wutz G, Nagasaka K, Tagoh H, Kostanova-Poliakova D, Schindler K, Sun Q, Bönelt P, Fischer M, Peters J-M, and Busslinger M. 2020. Wapl repression by Pax5 promotes V gene recombination by Igh loop extrusion. Nature 584: 142–147. [PubMed: 32612238]
8. Ba Z, Lou J, Ye AY, Dai H-Q, Dring EW, Lin SG, Jain S, Kyritsis N, Kieffer-Kwon K-R, Casellas R, and Alt FW. 2020. CTCF orchestrates long-range cohesin-driven V(D)J recombinational scanning. Nature 586: 305–310. [PubMed: 32717742]
9. Qiu X, Ma F, Zhao M, Cao Y, Shipp L, Liu A, Dutta A, Singh A, Braikia FZ, De S, Wood WH, Becker KG, Zhou W, Ji H, Zhao K, Atchison ML, and Sen R. 2020. Altered 3D chromatin structure permits inversional recombination at the IgH locus. Sci. Adv 6: eaaz8850. [PubMed: 32851160]
10. Dai H-Q, Hu H, Lou J, Ye AY, Ba Z, Zhang X, Zhang Y, Zhao L, Yoon HS, Chapdelaine-Williams AM, Kyritsis N, Chen H, Johnson K, Lin S, Conte A, Casellas R, Lee C-S, and Alt FW. 2021. Loop extrusion mediates physiological Igh locus contraction for RAG scanning. Nature 590: 338–343. [PubMed: 33442057]

11. Deriano L, Chaumeil J, Coussens M, Multani A, Chou Y, V Alekseyenko A, Chang S, Skok JA, and Roth DB. 2011. The RAG2 C terminus suppresses genomic instability and lymphomagenesis. Nature 471: 119–123. [PubMed: 21368836]
12. Helmink BA, and Sleckman BP. 2012. The Response to and Repair of RAG-Mediated DNA Double-Strand Breaks. Annu. Rev. Immunol 30: 175–202. [PubMed: 22224778]
13. Lee J, and Desiderio S. 1999. Cyclin A/CDK2 Regulates V(D)J Recombination by Coordinating RAG-2 Accumulation and DNA Repair. Immunity 11: 771–781. [PubMed: 10626899]
14. Brady BL, Steinel NC, and Bassing CH. 2010. Antigen Receptor Allelic Exclusion: An Update and Reappraisal. J. Immunol 185: 3801–3808. [PubMed: 20858891]
15. von Boehmer H, and Melchers F. 2010. Checkpoints in lymphocyte development and autoimmune disease. Nat. Immunol 11: 14–20. [PubMed: 20016505]
16. Zhang Y, Cheng TC, Huang G, Lu Q, Surleac MD, Mandell JD, Pontarotti P, Petrescu AJ, Xu A, Xiong Y, and Schatz DG. 2019. Transposon molecular domestication and the evolution of the RAG recombinase. Nature 569: 79–84. [PubMed: 30971819]
17. Bassing CH, Swat W, and Alt FW. 2002. The Mechanism and Regulation of Chromosomal V(D)J Recombination. Cell 109: 45–55.
18. Kumari G, and Sen R. 2015. Chromatin Interactions in the Control of Immunoglobulin Heavy Chain Gene Assembly. In Advances in Immunology 41–92.
19. Clark MR, Mandal M, Ochiai K, and Singh H. 2014. Orchestrating B cell lymphopoiesis through interplay of IL-7 receptor and pre-B cell receptor signalling. Nat. Rev. Immunol 14: 69–80. [PubMed: 24378843]
20. Johnson K, Hashimshony T, Sawai CM, Pongubala JMR, Skok JA, Aifantis I, and Singh H. 2008. Regulation of Immunoglobulin Light-Chain Recombination by the Transcription Factor IRF-4 and the Attenuation of Interleukin-7 Signaling. Immunity 28: 335–345. [PubMed: 18280186]
21. Mandal M, Okoreeh MK, Kennedy DE, Maienschein-Cline M, Ai J, McLean KC, Kaverina N, Veselits M, Aifantis I, Gounari F, and Clark MR. 2019. CXCR4 signaling directs Igk recombination and the molecular mechanisms of late B lymphopoiesis. Nat. Immunol 20: 1393–1403. [PubMed: 31477919]
22. Karki S, Banerjee S, Mclean K, Dinner A, and Clark MR. 2019. Transcription factories in Igκ allelic choice and diversity. Adv. Immunol 141: 33–49. [PubMed: 30904132]
23. Shinoda K, Maman Y, Canela A, Schatz DG, Livak F, and Nussenzweig A. 2019. Intra-Vκ Cluster Recombination Shapes the Ig Kappa Locus Repertoire. Cell Rep. 29: 4471–4481.e6. [PubMed: 31875554]
24. Nemazee D 2006. Receptor editing in lymphocyte development and central tolerance. Nat. Rev. Immunol 6: 728–740. [PubMed: 16998507]
25. Casellas R, Zhang Q, Zheng NY, Mathias MD, Smith K, and Wilson PC. 2007. Igκ allelic inclusion is a consequence of receptor editing. J. Exp. Med 204: 153–160. [PubMed: 17210730]
26. Mostoslavsky R, Alt FW, and Rajewsky K. 2004. Enigma of Allelic Exclusion Mechanism. Cell 118: 539–544. [PubMed: 15339659]
27. Vettermann C, and Schlissel MS. 2010. Allelic exclusion of immunoglobulin genes: Models and mechanisms. Immunol. Rev 237: 22–42. [PubMed: 20727027]
28. Mostoslavsky R, Singh N, Tenzen T, Goldmit M, Gabay C, Elizur S, Qi P, Reubinoff BE, Chess A, Cedar H, and Bergman Y. 2001. Asynchronous replication and allelic exclusion in the immune system. Nature 414: 221–225. [PubMed: 11700561]
29. Farago M, Rosenbluh C, Tevlin M, Fraenkel S, Schlesinger S, Masika H, Gouzman M, Teng G, Schatz D, Rais Y, Hanna JH, Mildner A, Jung S, Mostoslavsky G, Cedar H, and Bergman Y. 2012. Clonal allelic predetermination of immunoglobulin-κ rearrangement. Nature 490: 561–565. [PubMed: 23023124]
30. Levin-Klein R, Fraenkel S, Lichtenstein M, Matheson LS, Bartok O, Nevo Y, Kadener S, Corcoran AE, Cedar H, and Bergman Y. 2017. Clonally stable Vκ allelic choice instructs Igκ repertoire. Nat. Commun 8: 15575. [PubMed: 28555639]
31. Karki S, Kennedy DE, Mclean K, Grzybowski AT, Maienschein-Cline M, Banerjee S, Xu H, Davis E, Mandal M, Labno C, Powers SE, Le Beau MM, Dinner AR, Singh H, Ruthenburg

AJ, and Clark MR. 2018. Regulated Capture of Vκ Gene Topologically Associating Domains by Transcription Factories. Cell Rep. 24: 2443–2456. [PubMed: 30157436]

32. Alt FW, Enea V, Bothwell ALM, and Baltimore D. 1980. Activity of multiple light chain genes in murine myeloma cells producing a single, functional light chain. Cell 21: 1–12. [PubMed: 6773666]
33. Steinel NC, Lee B-S, Tubbs AT, Bednarski JJ, Schulte E, Yang-Iott KS, Schatz DG, Sleckman BP, and Bassing CH. 2013. The Ataxia Telangiectasia mutated kinase controls Igκ allelic exclusion by inhibiting secondary Vκ-to-Jκ rearrangements. J. Exp. Med 210: 233–239. [PubMed: 23382544]
34. Bredemeyer AL, Sharma GG, Huang CY, Helmink BA, Walker LM, Khor KC, Nuskey B, Sullivan KE, Pandita TK, Bassing CH, and Sleckman BP. 2006. ATM stabilizes DNA double-strand-break complexes during V(D)J recombination. Nature 442: 466–470. [PubMed: 16799570]
35. Callén E, Jankovic M, Difilippantonio S, Daniel JA, Chen H-T, Celeste A, Pellegrini M, McBride K, Wangsa D, Bredemeyer AL, Sleckman BP, Ried T, Nussenzweig M, and Nussenzweig A. 2007. ATM prevents the persistence and propagation of chromosome breaks in lymphocytes. Cell 130: 63–75. [PubMed: 17599403]
36. Helmink BA, Tubbs AT, Dorsett Y, Bednarski JJ, Walker LM, Feng Z, Sharma GG, McKinnon PJ, Zhang J, Bassing CH, and Sleckman BP. 2011. H2AX prevents CtIP-mediated DNA end resection and aberrant repair in G1-phase lymphocytes. Nature 469: 245–250. [PubMed: 21160476]
37. Steinel NC, Fisher MR, Yang-Iott KS, and Bassing CH. 2014. The Ataxia Telangiectasia Mutated and Cyclin D3 Proteins Cooperate To Help Enforce TCRβ and IgH Allelic Exclusion. J. Immunol 193: 2881–2890. [PubMed: 25127855]
38. Bredemeyer AL, Helmink BA, Innes CL, Calderon B, McGinnis LM, Mahowald GK, Gapud EJ, Walker LM, Collins JB, Weaver BK, Mandik-Nayak L, Schreiber RD, Allen PM, May MJ, Paules RS, Bassing CH, and Sleckman BP. 2008. DNA double-strand breaks activate a multi-functional genetic program in developing lymphocytes. Nature 456: 819–823. [PubMed: 18849970]
39. Bednarski JJ, Nickless A, Bhattacharya D, Amin RH, Schlissel MS, and Sleckman BP. 2012. RAG-induced DNA double-strand breaks signal through Pim2 to promote pre–B cell survival and limit proliferation. J. Exp. Med 209: 11–17. [PubMed: 22201128]
40. Bednarski JJ, Pandey R, Schulte E, White LS, Chen B-R, Sandoval GJ, Kohyama M, Haldar M, Nickless A, Trott A, Cheng G, Murphy KM, Bassing CH, Payton JE, and Sleckman BP. 2016. RAG-mediated DNA double-strand breaks activate a cell type–specific checkpoint to inhibit pre–B cell receptor signals. J. Exp. Med 213: 209–223. [PubMed: 26834154]
41. Arya R, and Bassing CH. 2017. V(D)J Recombination Exploits DNA Damage Responses to Promote Immunity. Trends Genet. 33: 479–489. [PubMed: 28532625]
42. Israël A 2010. The IKK complex, a central regulator of NF-kappaB activation. Cold Spring Harb. Perspect. Biol 2: 1–14.
43. Shih VFS, Tsui R, Caldwell A, and Hoffmann A. 2011. A single NFκB system for both canonical and non-canonical signaling. Cell Res. 21: 86–102. [PubMed: 21102550]
44. Hinz M, and Scheidereit C. 2014. The IκB kinase complex in NF-κB regulation and beyond. EMBO Rep. 15: 46–61. [PubMed: 24375677]
45. Fisher MR, Bassing CH, Schatz DG, Bloch NB, and Rivera-Reyes A. 2017. Immature Lymphocytes Inhibit Rag1 and Rag2 Transcription and V(D)J Recombination in Response to DNA Double-Strand Breaks. J. Immunol 198: 2943–2956. [PubMed: 28213501]
46. Kohyama M, Ise W, Edelson BT, Wilker PR, Hildner K, Mejia C, Frazier WA, Murphy TL, and Murphy KM. 2009. Role for Spi-C in the development of red pulp macrophages and splenic iron homeostasis. Nature 457: 318–321. [PubMed: 19037245]
47. Mombaerts P, Iacomini J, Johnson RS, Herrup K, Tonegawa S, and Papaioannou VE. 1992. RAG-1-deficient mice have no mature B and T lymphocytes. Cell 68: 869–877. [PubMed: 1547488]
48. Schmidt-Supprian M, Bloch W, Courtois G, Addicks K, Israël A, Rajewsky K, and Pasparakis M. 2000. NEMO/IKKγ-Deficient Mice Model Incontinentia Pigmenti. Mol. Cell 5: 981–992. [PubMed: 10911992]
49. Derudder E, Cadera EJ, Vahl JC, Wang J, Fox CJ, Zha S, van Loo G, Pasparakis M, Schlissel MS, Schmidt-Supprian M, Rajewsky K, Vahl C, Wang J, Fox CJ, Zha S, van Loo G, Pasparakis

M, Schlissel MS, Schmidt-Supprian M, and Rajewsky K. 2009. Development of immunoglobulin λ-chain–positive B cells, but not editing of immunoglobulin κ-chain, depends on NF-κB signals. Nat. Immunol 10: 647–654. [PubMed: 19412180]

50. Ochodnicka-Mackovicova K, Bahjat M, Maas C, van der Veen A, Bloedjes TA, de Bruin AM, van Andel H, Schrader CE, Hendriks RW, Verhoeyen E, Bende RJ, van Noesel CJM, and Guikema JEJ. 2016. The DNA Damage Response Regulates RAG1/2 Expression in Pre-B Cells through ATM-FOXO1 Signaling. J. Immunol 197: 2918–29. [PubMed: 27559048]
51. Gapud EJ, Dorsett Y, Yin B, Callen E, Bredemeyer A, Mahowald GK, Omi KQ, Walker LM, Bednarski JJ, McKinnon PJ, Bassing CH, Nussenzweig A, and Sleckmana BP. 2011. Ataxia telangiectasia mutated (Atm) and DNA-PKcs kinases have overlapping activities during chromosomal signal joint formation. Proc. Natl. Acad. Sci. U. S. A 108: 2022–2027. [PubMed: 21245316]
52. Casellas R, Shih Tien-An Yang, Kleinewietfeld M, Rakonjac J, Nemazee D, Rajewsky K, and Nussenzweig MC. 2001. Contribution of receptor editing to the antibody repertoire. Science (80-.). 291: 1541–1544.
53. Hewitt SL, Yin B, Ji Y, Chaumeil J, Marszalek K, Tenthorey J, Salvagiotto G, Steinel N, Ramsey LB, Ghysdael J, Farrar MA, Sleckman BP, Schatz DG, Busslinger M, Bassing CH, and Skok JA. 2009. RAG-1 and ATM coordinate monoallelic recombination and nuclear positioning of immunoglobulin loci. Nat. Immunol 10: 655–64. [PubMed: 19448632]
54. Hewitt SL, Wong JB, Lee JH, Nishana M, Chen H, Coussens M, Arnal SM, Blumenberg LM, Roth DB, Paull TT, and Skok JA. 2017. The Conserved ATM Kinase RAG2-S365 Phosphorylation Site Limits Cleavage Events in Individual Cells Independent of Any Repair Defect. Cell Rep. 21: 979–993. [PubMed: 29069605]
55. Rodgers W, Byrum JN, Sapkota H, Rahman NS, Cail RC, Zhao S, Schatz DG, and Rodgers KK. 2015. Spatio-temporal regulation of RAG2 following genotoxic stress. DNA Repair (Amst). 27: 19–27. [PubMed: 25625798]
56. Brecht RM, Liu CC, Beilinson HA, Khitun A, Slavoff SA, and Schatz DG. 2020. Nucleolar localization of RAG1 modulates V(D)J recombination activity. Proc. Natl. Acad. Sci. U. S. A 117: 4300–4309. [PubMed: 32047031]
57. Wu Z-H, Shi Y, Tibbetts RS, Miyamoto S, and S. Wu Z-H; Shi Yuling; Tibbetts Randal S.; Miyamoto. 2006. Molecular Linkage Between the Kinase ATM and NF- B Signaling in Response to Genotoxic Stimuli. Science (80-.). 311: 1141–1146.
58. Stilmann M, Hinz M, Arslan SC, Zimmer A, Schreiber V, and Scheidereit C. 2009. A nuclear poly(ADP-ribose)-dependent signalosome confers DNA damage-induced IkappaB kinase activation. Mol. Cell 36: 365–78. [PubMed: 19917246]
59. Hinz M, Stilmann M, Arslan SÇ, Khanna KK, Dittmar G, and Scheidereit C. 2010. A cytoplasmic ATM-TRAF6-cIAP1 module links nuclear DNA damage signaling to ubiquitin-mediated NF-κB activation. Mol. Cell 40: 63–74. [PubMed: 20932475]
60. Sabatel H, Di Valentin E, Gloire G, Dequiedt F, Piette J, and Habraken Y. 2012. Phosphorylation of p65(RelA) on Ser547 by ATM Represses NF-κB-Dependent Transcription of Specific Genes after Genotoxic Stress. PLoS One 7: e38246. [PubMed: 22715377]
61. Zhao M, Joy J, Zhou W, De S, Wood WH, Becker KG, Ji H, and Sen R. 2018. Transcriptional outcomes and kinetic patterning of gene expression in response to NF-κB activation. PLOS Biol. 16: e2006347. [PubMed: 30199532]
62. Amin RH, and Schlissel MS. 2008. Foxo1 directly regulates the transcription of recombination-activating genes during B cell development. Nat. Immunol 9: 613–622. [PubMed: 18469817]

Key Points

1. Nemo deficiency impairs RAG DSB signaling without affecting RAG DSB repair.
2. Nemo deficiency allows bi-allelic RAG cleavage and surface expression of *Igk* loci.
3. Nemo-dependent, ATM-mediated RAG DSB signaling enforces Igκ allelic exclusion.

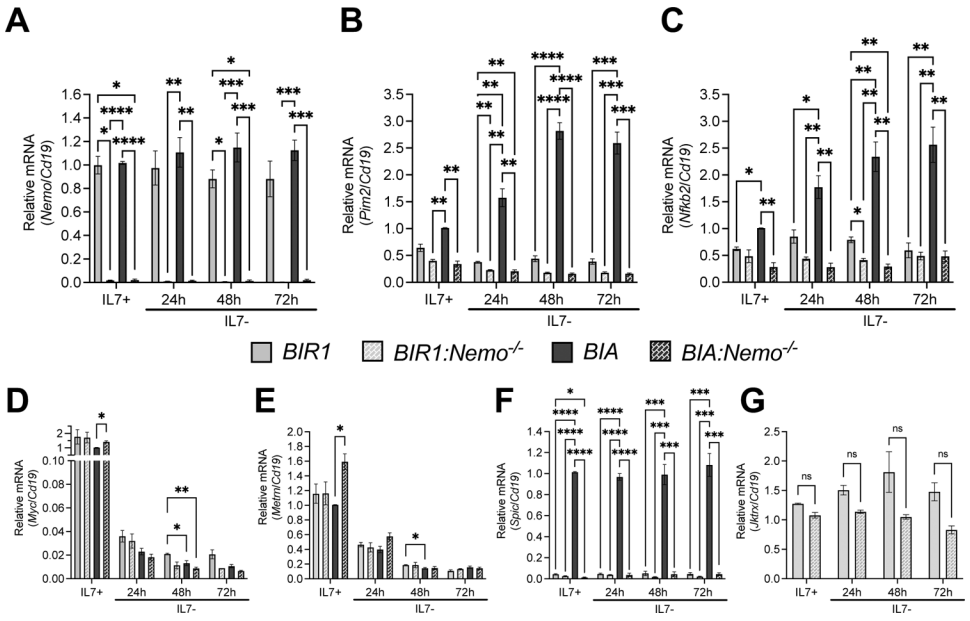

FIGURE 1.

B lineage conditional inactivation of Nemo disrupts RAG DSB-induced gene expression changes in pre-B cells. (***A-F***) qRT-PCR quantification of (**A**) *Nemo*, (**B**) *Pim2*, (**C**) *Nfkb2*, (**D**) *Myc*, (**E**) *Metrn*, (**F**) *Spic*, and (**G**) germline J_k (*Jktrx*) transcripts in primary pre-B cell cultures from *BCL2:IgH:Rag1*$^{-/-}$*:Nemo*$^{flox/flox}$ (*BIR1*), *Mb1Cre*$^{+}$*:BCL2:IgH:Rag1*$^{-/-}$*:Nemo*$^{flox/flox}$ (*BIR1:Nemo*$^{-/-}$), *BCL2:IgH:Artemis*$^{-/-}$*:Nemo*$^{flox/flox}$ (*BIA*), or *Mb1Cre*$^{+}$*:BCL2:IgH:Artemis*$^{-/-}$*:Nemo*$^{flox/flox}$ (*BIA:Nemo*$^{-/-}$) mice. Cells were collected after culturing in the presence of IL7 for 4 days or then 24, 48, or 72 hours after IL7 withdrawal. These data represent the mean value of the replicates (*BIR1*, n=3; *BIR1:Nemo*$^{-/-}$, n=3; *BIA*, n=6; *BIA:Nemo*$^{-/-}$, n=4) +/− SEM from six independent experiments that each included a *BIA* culture to normalize data. Each transcript was first normalized to *Cd19* to account for cDNA input and then normalized to the *BIA* IL7^{+} sample. Statistical significance determined by Two-way ANOVA and Tukey's post-tests for multiple comparisons (ns, not significant; *, <0.0332; **, <0.0021; ***, <0.0002; ****, <0.0001).

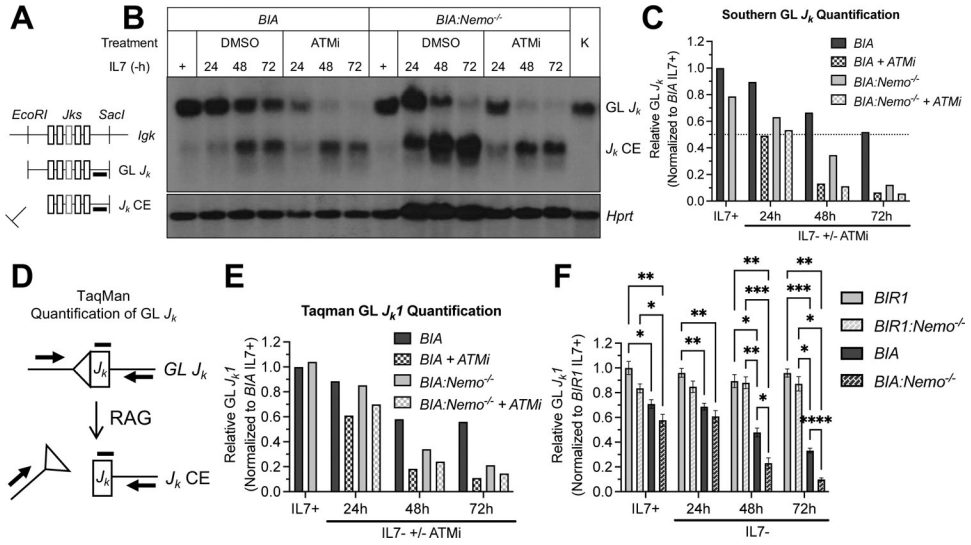

FIGURE 2.

Nemo inactivation leads to increased RAG cleavage of *Igk* loci. (**A**) Schematic for Southern analysis of *Igk* cleavage by RAG indicating the germline (GL) configuration of the J_k region of the *Igk* locus with flanking *EcoRI and SacI* restriction sites, the GL *Jk* region generated by *EcoR1* and *SacI* digestion, and each J_k coding end (CE) generated by RAG cleavage. (**B**) Representative Southern blot analysis of J_k cleavage and (**C**) quantification of the remaining GL J_k fragment in primary pre-B cell cultures from *BCL2:IgH:Artemis*$^{-/-}$*:Nemo*$^{flox/flox}$ (*BIA*) and *Mb1Cre*$^{+}$*:BCL2:IgH:Artemis*$^{-/-}$*:Nemo*$^{flox/flox}$ (*BIA:Nemo*$^{-/-}$) mice. Cells were collected after 4 days of culture in IL7 or at 24, 48, or 72 hours after IL7 withdrawal of cultures treated with or without the ATM inhibitor (ATMi) KU55933 (15uM). The probe 3' of the J_k region depicts the GL J_k fragment and indicated J_k CEs. Southern blot using a probe for *Hprt* was used to normalize DNA content in each lane. The quantification is the amount of GL J_k relative to *Hprt* and normalized to the *BIA* IL7^{+} sample. These data are from one independent experiment. (**D**) Schematic of Taqman quantification of GL J_k indicating the relative positions of the primers and Taqman probe used for each J_k gene segment. (**E**) Taqman quantification of GL J_k1 from the same samples as the ones used for the Southern blot analysis in B and C. Taqman quantification of the *Cd19* locus was used to normalize DNA content. The J_k1 value was first normalized to *Cd19* and then to the *BIA* IL7^{+} sample. These data are from one independent experiment. (**F**) Taqman quantification of GL J_k1 from an aliquot of the same samples as Figure 1. These samples are from primary pre-B cell cultures from *BCL2:IgH:Rag1*$^{-/-}$*:Nemo*$^{flox/flox}$ (*BIR1*), *Mb1Cre*$^{+}$*:BCL2:IgH:Rag1*$^{-/-}$*:Nemo*$^{flox/flox}$ (*BIR1:Nemo*$^{-/-}$), *BCL2:IgH:Artemis*$^{-/-}$*:Nemo*$^{flox/flox}$ (*BIA*) and *Mb1Cre*$^{+}$*:BCL2:IgH:Artemis*$^{-/-}$*:Nemo*$^{flox/flox}$ (*BIA:Nemo*$^{-/-}$) mice after 4 days of culture in IL7 or at 24, 48, or 72 hours after IL7 withdrawal. J_k1 values were normalized to *Cd19* for DNA content and normalized to the *BIR1* IL7^{+} sample. The bars represent the mean value of the replicates (*BIR1*, n=3; *BIR1:Nemo*$^{-/-}$, n=3; *BIA*, n=6; *BIA:Nemo*$^{-/-}$, n=4) from six independent experiments +/− SEM. Statistical significance determined by Two-way ANOVA and Tukey's post-tests for multiple comparisons (*, <0.0332; **, <0.0021; ***, <0.0002; ****, <0.0001).

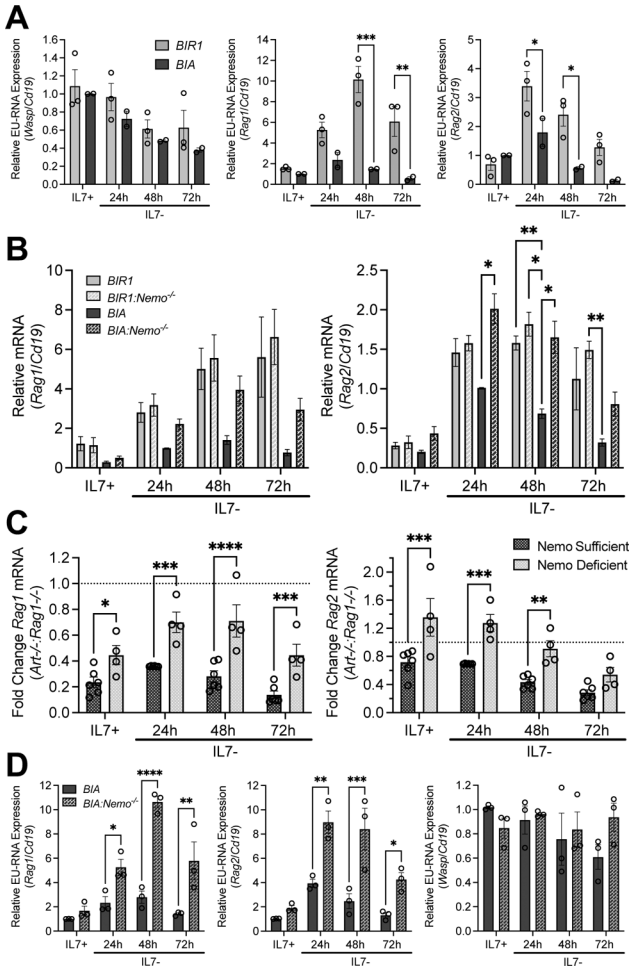

FIGURE 3.

Nemo inactivation impairs RAG DSB-triggered transcriptional downregulation of *Rag1* and *Rag2* expression. (**A**) qRT-PCR quantification of EU-labelled *Wasp*, *Rag1*, and *Rag2* transcripts in primary pre-B cell cultures from *BCL2:IgH:Rag1*$^{-/-}$*:Nemo*$^{flox/flox}$ (*BIR1*) and *BCL2:IgH:Artemis*$^{-/-}$*:Nemo*$^{flox/flox}$ (*BIA*) mice after 4 days in IL7 or 24, 48, or 72 hours after IL7 withdrawal. The value for each transcript was calculated relative to *Cd19* and normalized to the *BIA* IL7^{+} sample. Individual points indicate replicates (*BIR1*, n=3; *BIA*, n=2) from two independent experiments. (**B**) qRT-PCR quantification of steady state levels of *Rag1* and *Rag2* transcripts from the same samples analyzed in Figure 1. These are samples from primary pre-B cell cultures from *BIR1*, *Mb1Cre*$^{+}$*:BCL2:IgH:Rag1*$^{-/-}$*:Nemo*$^{flox/flox}$ (*BIR1:Nemo*$^{-/-}$), *BIA*, and *Mb1Cre*$^{+}$*:BCL2:IgH:Artemis*$^{-/-}$*:Nemo*$^{flox/flox}$ (*BIA:Nemo*$^{-/-}$) mice. Cells were collected after culturing in IL7 for 4 days or then 24, 48, or 72 hours after IL7 withdrawal. Each transcript was first normalized to *Cd19* to account for cDNA input and then normalized to the *BIA* 24h IL7^{-} sample. These data represent the mean value of the replicates (*BIR1*, n=3; *BIR1:Nemo*$^{-/-}$, n=3; *BIA*, n=6; *BIA:Nemo*$^{-/-}$, n=4) +/− SEM from six independent experiments that each included a *BIA* culture to normalize the data. (**C**) The same qRT-PCR quantification of *Rag1* and *Rag2* steady state levels as B, but presented

as the fold change ratio of relative levels of each transcript in cells with RAG DSBs (*Art*$^{-/-}$) to cells without RAG DSBs (*Rag1*$^{-/-}$) that are either Nemo-sufficient (*BIA*/*BIR1*) or Nemo-deficient (*BIA:Nemo*$^{-/-}$/*BIR1:Nemo*$^{-/-}$). The dotted line represents a value of 1, which would indicate that RAG DSBs had no effect on the level of each transcript, while values below 1 indicate RAG DSB-induced repression. Each point represents a ratio calculated using an individual replicate of *BIA* or *BIA:Nemo*$^{-/-}$ and the average *BIR1* or *BIR1:Nemo*$^{-/-}$ value at each time point. The bars represent the mean value of the ratios +/− SEM. (**D**) qRT-PCR quantification of EU-labelled *Rag1*, *Rag2* and *Wasp* transcript levels in primary pre-B cell cultures from *BIA* and *BIA:Nemo*$^{-/-}$ mice after 4 days in IL7 or 24, 48, and 72 or after IL7 withdrawal. The value for each transcript was calculated relative to *Cd19* and normalized to the *BIA* IL7^{+} sample. Individual points indicate replicates (*BIA*, n=3; *BIA:Nemo*$^{-/-}$, n=3) from three independent experiments. Statistical significance determined by Two-way ANOVA and Tukey's post-tests for multiple comparisons (*, <0.0332; **, <0.0021; ***, <0.0002; ****, <0.0001).

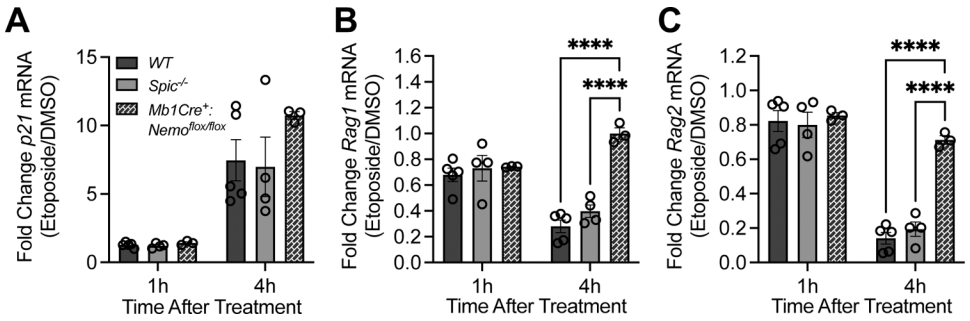

FIGURE 4.

Inactivation of Nemo but not SpiC impairs genotoxic DSB-induced repression of *Rag1* and *Rag2* transcripts. (**A-C**) qRT-PCR quantification of (**A**) *p21*, (**B**) *Rag1*, and (**C**) *Rag2* mRNA in total bone marrow from wild-type (*WT*), *Spic*$^{-/-}$, and *Mb1Cre*$^{+}$*:Nemo*$^{flox/flox}$ mice. Bone marrow from individual mice were treated with etoposide (10μg/mL) or DMSO and collected 1 or 4 hours after treatment. The value for each transcript was calculated relative to *Cd19* and normalized to the baseline sample for each individual mouse. The data are presented as fold change ratios of relative levels of each transcript in etoposide treated cells compared with DMSO treated cells at 1 or 4 hours after treatment. Individual points indicate replicates (*WT*, n=5; *Spic*$^{-/-}$, n=4; *Mb1Cre*$^{+}$*:Nemo*$^{-/-}$, n=3) from two independent experiments and bars represent the mean +/− SEM. Statistical significance determined by Two-way ANOVA and Tukey's post-tests for multiple comparisons (*, <0.0332; **, <0.0021; ***, <0.0002; ****, <0.0001).

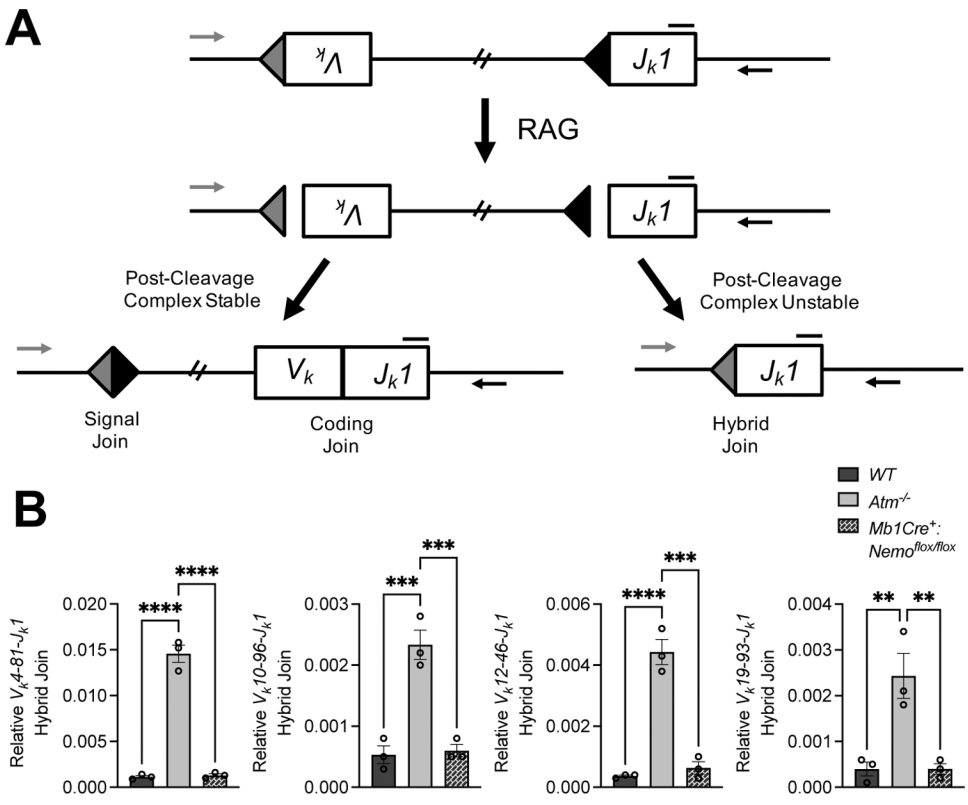

FIGURE 5.

Nemo inactivation does not increase hybrid joins formed by inversional *Igk* rearrangements. (**A**) Schematic of a V_k-to-J_k1 inversional rearrangement indicating an example V_k gene segment that has the potential to rearrange by inversion to J_k1 and the relative position of the Taqman primers and probe used to quantify the hybrid join. (**B**) Taqman quantification of hybrid joins generated from RAG cleavage at $V_k4–81$, $V_k10–96$, $V_k12–46$, or $V_k19–93$ and J_k1 in pre-B cells (single, live, B220$^+$:CD43$^-$:IgM$^-$) sorted from the bone marrow of *WT*, *Atm*$^{-/-}$, and *Mb1Cre*$^+$*:Nemo*$^{flox/flox}$ mice. Hybrid join levels were calculated relative to the *Cd19* locus to account for DNA content. Individual points indicate replicates (all genotypes, n=3) from two independent flow cytometry sorts and the bars represent the mean value +/− SEM. Statistical significance determined by One-way ANOVA and Tukey's post-tests for multiple comparisons (*, <0.0332; **, <0.0021; ***, <0.0002; ****, <0.0001).

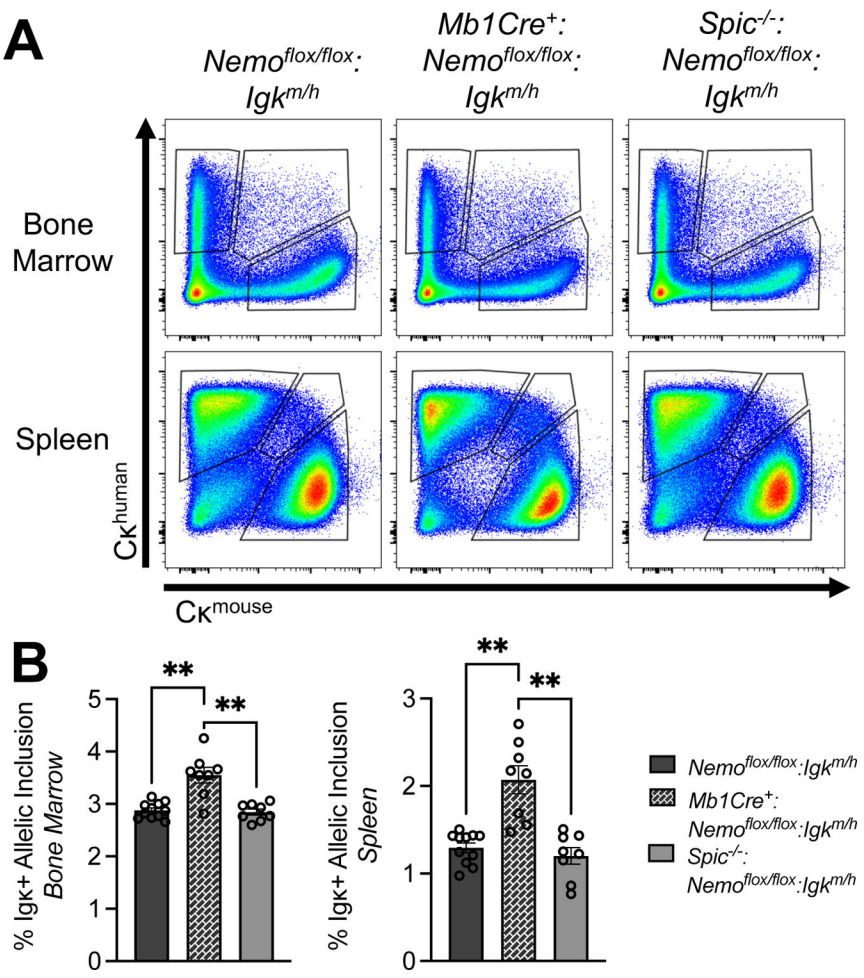

FIGURE 6.

Inactivation of Nemo but not SpiC increases bi-allelic Igκ protein expression. (**A**) Representative plots of B220^{+}:CD43^{-} cells that express Igκ$^{\text{human(h)}}$, Igκ$^{\text{mouse(m)}}$, or both Igκ$^{\text{h}}$ and Igκ$^{\text{m}}$ from the bone marrow or spleen of *Nemo$^{flox/flox}$:Igk$^{m/h}$*, *Mb1Cre^{+}:Nemo$^{flox/flox}$:Igk$^{m/h}$*, and *Spic$^{-/-}$:Nemo$^{flox/flox}$:Igk$^{m/h}$* mice. (**B**) Quantification of the frequency of Igκ allelic inclusion that was calculated by dividing the frequency of Igκ$^{\text{h+ and m+}}$ cells by the frequency of total Igκ^{+} cells. Individual points represent replicates (*Nemo$^{flox/flox}$:Igk$^{m/h}$*, n=11; *Mb1Cre^{+}:Nemo$^{flox/flox}$:Igk$^{m/h}$*, n=8; *Spic$^{-/-}$:Nemo$^{flox/flox}$:Igk$^{m/h}$*, n=8) from nine independent experiments and bars represent the mean +/− SEM. Statistical significance determined by Brown-Forsythe and Welch ANOVA and Dunnett T3 post-tests for multiple comparisons (*, <0.0332; **, <0.0021; ***, <0.0002; ****, <0.0001).